J|A|C|S ARTICLES

Published on Web 09/29/2010

DFT Study of the Structure and Reactivity of the Terminal Pt(IV)-Oxo Complex Bearing No Electron-Withdrawing Ligands

Irena Efremenko, Elena Poverenov, Jan M. L. Martin,* and David Milstein*

Department of Organic Chemistry, Weizmann Institute of Science, Rehovot 76000, Israel

Received June 23, 2010; E-mail: gershom@weizmann.ac.il; david.milstein@weizmann.ac.il

Abstract: The recently published $[(PCN)Pt{=}O]^+$ complex is interesting as a unique example of a stable d^6 terminal transition metal oxo complex not stabilized by electron withdrawing ligands and as a model of oxo complexes frequently implicated as key intermediates in various processes of oxygen transfer. In the present work, we report an extensive DFT study of its geometric and electronic structure, composition in solution, and reactivity. The thermodynamic data and calculated ^{195}Pt NMR chemical shifts reveal that one solvent molecule is weakly coordinated to the complex in acetone solution. This ancillary ligand is responsible for the diamagnetic state of the complex, retards intramolecular oxygen transfer, and facilitates CO oxidation. Chemical transformations of the coordinated acetone molecule, coordination of other ancillary ligands present in the reaction mixture, and protonation of the Pt-oxo group in nonacidic media are excluded based on thermodynamic or kinetic considerations. Bonding of the terminal oxo ligand with strong electrophiles presents the key interaction in the mechanisms of intramolecular oxygen insertion into the Pt−P bond, in CO oxidation and in water activation mediated by microsolvation. Low affinity of the terminal oxo ligand toward "soft" covalent interactions brings about intermediate formation of agostic hydrido and hydroxo complexes along the reaction pathway of dihydrogen oxidation. Stabilization of the Pt-oxo bonding is attributed to bending of the terminal oxo ligand out of the plane of the complex and to significant transfer of electron density from compact low lying Pt 5d orbitals to more diffuse 6s and 6p orbitals.

1. Introduction

Terminal metal oxo complexes have long been invoked as key intermediates in various biological, homogeneous and heterogeneous catalytic oxidation processes, in which O transfer takes place, as well as in oxygen activation or oxygen generation on transition metal surfaces.[1] Terminal oxo complexes of transition metals with no more than four d electrons are quite stable and common.[2] However, despite numerous efforts, until recently there was no evidence for the existence of late transition metal oxo complexes with *d* electron count larger than four. The instability of these complexes arises from π antibonding, playing a critical role in electron-rich complexes.[3] From Scheme 1, one can see that π^* orbitals become occupied in $d^{>2}$ octahedral complexes and in $d^{>4}$ square planar complexes. Reduction of the excessive electron density by π backdonation strengthens the TM=O bond (TM = transition metal). Thus, rare examples of d^6 TM oxo complexes stabilized by electron withdrawing frameworks have been recently isolated.

In our previous publication,[5] we reported the first d^6 terminal Pt oxo complex not stabilized by electron withdrawing ligands, synthesized by treatment of the pincer PCN-Pt complex **1A** with dimethyl dioxirane, a strong oxidizing agent (reaction 1 in Scheme 2). DFT calculations showed that the reaction is moderately exergonic ($\Delta G^0_{298} = -10.8$ kcal mol^{-1} in absence of ancillary ligands and -5.31 kcal mol^{-1} in presence of coordinated acetone) and that the bulky P(*t*-Bu)$_2$ group prevents complex **2** from dimerization with formation of a more common dimeric $[(PCN)Pt(\mu\text{-}O)]_2$ structure. Complex **2** showed diverse

(1) (a) Nugent, W. A.; Mayer, J. M. *Metal-Ligand Multiple Bonds*; Wiley: New York, 1988. (b) Holm, R. H. *Chem. Rev.* **1987**, *87*, 1401–1449. (c) Sheldon, R. A.; Kochi, J. K. *Metal-Catalyzed Oxidations of Organic Compounds*; Academic Press: New York, 1981. (d) *Biomimetic Oxidations Catalyzed by Transition Metal Complexes*; Meunier, B., Ed.; Imperial College Press: London, 2000. (e) Yoshizawa, K. *Acc. Chem. Res.* **2006**, *39*, 375–382. (f) Rohde, J.-U.; In, J.-H.; Lim, M. H.; Brennessel, W. W.; Bukowski, M. R.; Stubna, A.; Munk, E.; Nam, W.; Que, L., Jr. *Science* **2003**, *299*, 1037–1039. (g) Green, M. T.; Dawson, J. H.; Gray, H. B. *Science* **2004**, *304*, 1653–1656. (h) Somorjai, G. A. *Introduction to Surface Chemistry and Catalysis*; Wiley: New York, 1994. (i) Ruettinger, W.; Dismukes, G. C. *Chem. Rev.* **1997**, *97*, 1–24. (j) Yagi, M.; Kaneko, M. *Chem. Rev.* **2001**, *101*, 21–35. (k) Alstrum-Acevedo, J. H.; Brennaman, M. K.; Meyer, T. J. *Inorg. Chem.* **2005**, *44*, 6802–6827. (l) Dempsey, J. L.; Esswein, A. J.; Manke, D. R.; Rosenthal, J.; Soper, J. K.; Nocera, D. G. *Inorg. Chem.* **2005**, *44*, 6879–6892. (m) Lewis, N. S.; Nocera, D. G. *Proc. Natl. Acad. Sci. U.S.A.* **2006**, *103*, 15729–15735.

(2) For review, see, for example: (a) Kühn, F. E.; Herrmann, W. A. *Struct. Bonding (Berlin)* **2000**, *97*, 213–236. (b) Griffith, W. P. *Coord. Chem. Rev.* **1970**, *5*, 359. (c) Griffith, W. P. *Trans. Met. Chem.* **1990**, *15*, 251. (d) Porai-Koshits, M. A.; Sergienko, V. S. *Russ. Chem. Rev.* **1990**, *59*, 52–62.

(3) (a) Cartert, E. A.; Goddard, W. A. *J. Phys. Chem.* **1988**, *92*, 2109–2115. (b) Mayer, J. M. *Comm. Inorg. Chem.* **1988**, *8*, 125–135. (c) Parkin, G. *Prog. Inorg. Chem.* **1998**, *47*, 1.

(4) (a) Anderson, T. M.; Neiwert, W. A.; Kirk, M. L.; Piccoli, P. M. B.; Schultz, A. J.; Koetzle, T. F.; Musaev, D. G.; Morokuma, K.; Cao, R.; Hill, C. L. *Science* **2004**, *306*, 2074–2077. (b) Anderson, T. M.; et al. *J. Am. Chem. Soc.* **2005**, *127*, 11948–11949. (c) Cao, R.; et al. *J. Am. Chem. Soc.* **2007**, *129*, 11118–11133. (d) Spaltenstein, E.; Conry, R. R.; Critchlow, S. C.; Mayer, J. M. *J. Am. Chem. Soc.* **1989**, *111*, 8741–8742. Ad5 Fe(III) terminal oxo complex stabilized by hydrogen bonding: (e) MacBeth, C. E.; Golombek, A. P.; Young, V. G., Jr; Yang, C.; Kuczera, K.; Hendrich, M. P.; Borovik, A. S. *Science* **2008**, *289*, 938–941.

(5) Poverenov, E.; Efremenko, I.; Frenkel, A. I.; Ben-David, Y.; Shimon, L. J. W.; Leitus, G.; Konstantinovski, L.; Martin, J. M. L.; Milstein, D. *Nature* **2008**, *455*, 1093–1096.

10.1021/ja105197x

Scheme 1. Qualitative Representation of d Orbital Splitting Induced by Occupied p_π Orbitals of an Oxygen Ligand in Octahedral (Left) and Square Planar (Right) d^6 Complexes[a]

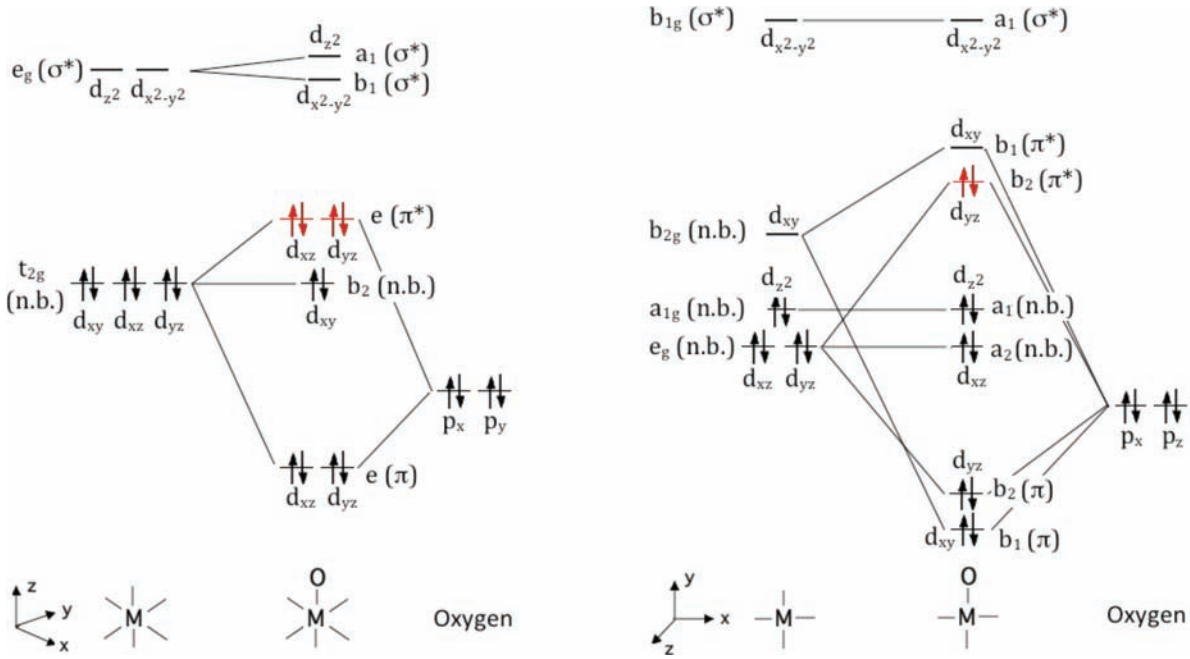

[a] Occupied π^* orbitals responsible for instability of late transition metal complexes are highlight in red.

Scheme 2. Formation and Reactivity of Pt-Oxo Complex **2**

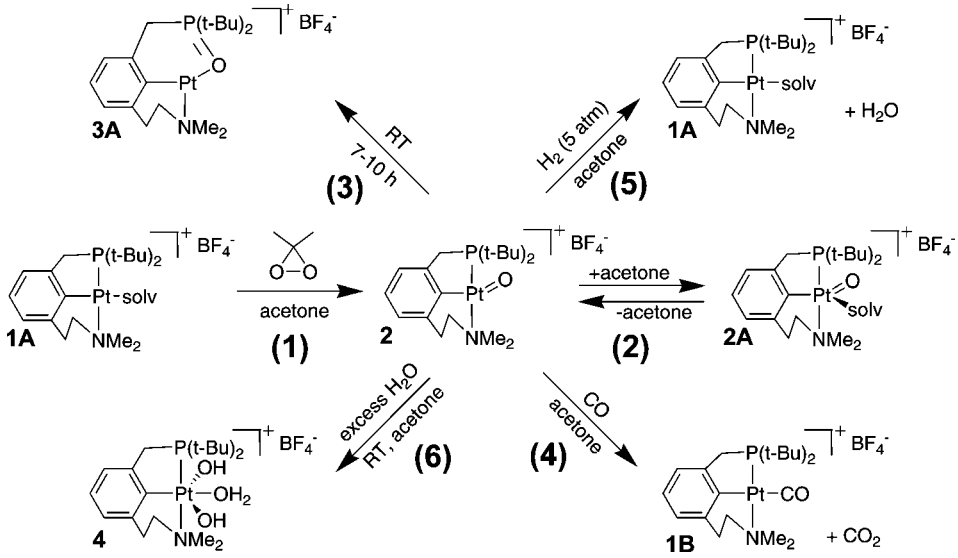

reactivity (reactions 3−6 in Scheme 2), shedding light on mechanisms of catalytic reactions, in which formation of a terminal late TM oxo intermediates might be involved.

In the present work, we extend the theoretical analysis of the structure and reactivity of the Pt-oxo complex. We were not able to isolate the compound in a single-crystal form suitable for X-ray and neutron diffraction studies. Thus, the first aim of this work is to explore the exact structure of the Pt-oxo complex **2** in solution by comparison of its calculated and experimentally observed properties. The second aim is detailed analysis of the mechanisms of oxygen transfer and water activation reactions. This can provide deeper insight into the chemical nature of electron rich terminal oxo complexes and their reactivity as intermediates in catalytic reactions. The third aim is to inquire into the electronic structure of the complex and to find out the reason for its surprising stability.

2. Computational Methods

Geometry optimization and evaluation of harmonic frequencies were performed at the density functional theory (DFT) level,[6] using the PBE0 hybrid density functional,[7] in conjunction with the PC-1 basis set. This basis set is a combination of Jensen's polarization consistent pc-1 basis set[8] for the main group elements and the relativistic energy-consistent pseudopotential (RECP) basis set SDD[9] for platinum, with an added f-type polarization exponent taken as the geometric average of the two f-exponents given by Martin and Sundermann.[10] This combination is of double-ζ plus polarization quality. The accuracy of the computational method in

(6) (a) Kohn, W.; Sham, L. J. *Phys. Rev.* **1965**, *140*, A1133–A1138. (b) Parr, R. G.; Yang, W. *Density Functional Theory of Atoms and Molecules*; Oxford University Press: New York, 1970; p 230.
(7) Adamo, C.; Cossi, M.; Barone, V. *J. Mol. Struct. (THEOCHEM)* **1999**, *493*, 145–157.

predicting the geometries of the experimental complexes was previously validated by calculating the geometry of complexes for which the crystal structure is known.[5] All structures were fully optimized in the gas phase and characterized as minima or transition states by calculating the harmonic vibrational frequencies. The connectivity of the transition states was confirmed by performing intrinsic reaction coordinate (IRC) calculations[11] with 10 points in each direction followed by full optimization of the resulting geometries. All DFT calculations were carried out using the Gaussian 03[12] and Gaussian 09[13] software packages.

Bulk solvent effects of the experimental acetone media have been taken into account via the self-consistent reaction field (SCRF) method, using the integral equation formalism polarizable continuum model (IEF-PCM)[14] as it is implemented in Gaussian 09 at the PBE0/AUG-PC1 level of theory. Dispersion interactions within the computed structures were also taken into account. These weak interactions determined by intramolecular van der Waals forces can amount to 10−20 kcal mol^{-1} in large complexes.[15] In the present work, these interactions are included by adding an empirical dispersion correction term, as was proposed by Schwabe and Grimme,[16] with a value $s_6 = 0.70$, as suggested by Karton et al. for the PBE0 functional.[17] Unless stated otherwise, energetic data are presented as free energies (ΔG) at 298.15 K in acetone solution, where $G = E_{\text{acetone}}(\text{PBE0/AUG-PC1}) + \Delta G_{\text{corr}}(\text{PBE0/PC1}) + E_{\text{vDW}}$. It differs from our previous work,[5] in which energetic data were obtained at the PBE0/PC1 level of theory and dispersion corrections were not taken into account.

NMR chemical shifts were obtained from gauge-including atomic orbitals (GIAO) calculations[18] at several theoretical levels. The ^{13}C and ^{1}H isotropic shifts were calculated using PBE0/PC-1 combination. Obtained values were transferred to chemical shifts δ comparable with the experimental measurements by two techniques. The first one consisted in calibration of calculated raw isotropic shifts σ with respect to ^{13}C and ^{1}H shifts in small molecules calculated at the CCSD(T) level and extrapolated to the complete basis set limit according to the equations: $\sigma_C' = 0.925\sigma_C + 8.313$ and $\sigma_H' = 0.942\sigma_H + 1.509$. Then ^{13}C and ^{1}H chemical shifts in tetramethylsilane (TMS) were calculated at the PBE0/PC-1 level of theory and scaled using the same equations. Finally, predicted chemical shifts δ were calculated from the scaled isotropic shifts σ' as $\delta = \sigma'_{\text{TMS}} - \sigma'$. According to the second technique, the calculated ^{13}C and ^{1}H isotropic shifts were scaled using the equations $\delta_C = -0.851*\sigma_C + 173.598$ and $\delta_H = -0.919*\sigma_H + 29.567$, predetermined from the dependence of experimental chemical shifts δ on raw calculated isotropic shifts σ for small molecules (see Supporting Information for further details).

The ^{195}Pt, ^{13}C, and ^{1}H chemical shifts were also calculated using the second-order Douglas-Kroll-Hess (DKH2) scalar relativistic approach[19] with the GGA density functional PBE[20] and with the hybrid GGA density functional PBE0. The segmented all-electron relativistically contracted (SARC) basis set on Pt[21] constructed for use in conjunction with the DKH Hamiltonian and triple-ζ valence (TZV) basis set of Karlsruhe group[22] reconstructed for DKH Hamiltonian[23] on others elements were applied in these calculations. In order to avoid convergence problems, the modest integral accuracy early in direct SCF, that is default in Gaussian09, was turned off; the "medium" (50 194) integration grid was used for the CPHF portion while the unpruned (140 590) grid was applied for the rest integrations in both PCM and GIAO calculations. The calculated values were scaled with respect to the corresponding chemical shifts experimentally measured for small molecules (see Supporting Information). In all GIAO calculations, the solvation effect was taken into account by IEF-PCM calculations at the same theoretical level.

Notation and References for Other Computational Methods Used. DFT methods: hybrid meta M06[24] and double hybrid B2GP-PLYP;[25] MP2 methods: unrestricted (UMP2) and restricted open shell (ROMP2); coupled cluster methods: CCSD(T) and CCSD[T]—coupled cluster with singles, doubles, and quasiperturbative triple excitations, AQCC—averaged quadratic coupled-cluster method.[26]

Notation for Other Basis Sets Used. AUG-PC1, PC2, and AUG-PC2 stand for combinations of the Jensen's polarization consistent aug-pc-1, pc2 and aug-pc2 basis sets on the main group elements,[8,27] with the SDD basis set[9] on platinum. To the latter, 1f, 2f1g+diffuse(spd), and 2f1g+diffuse(spdfg) functions were added. The polarization functions were taken from ref 10, while the *spd* diffuse functions were obtained for the purpose of this work by means of completeness profiles,[28] and the fg diffuse functions were optimized at the CISD level for the atomic anion. (The exponents are given in Supporting Information.) The spd/vdz, spd/vtz and spdf/vtz are correlation consistent cc-pVDZ, cc-pVTZ(no f) and cc-pVTZ(spdf) basis sets, respectively.

For qualitative interpretation of the computational results the PBE0/PC1 electron density of the complexes in optimized geom-

(8) (a) Jensen, F. *J. Chem. Phys.* **2001**, *115*, 9113–9125. (b) Jensen, F. *J. Chem. Phys.* **2002**, *116*, 7372–7379.
(9) Dolg, M. In *Modern Methods and Algorithms of Quantum Chemistry*; Grotendorst, J., Ed.; John von Neumann Institute for Computing: Jülich, Germany, 2000; Vol. 1, pp 479−508.
(10) Martin, J. M. L.; Sundermann, A. *J. Chem. Phys.* **2001**, *114*, 3408–3420.
(11) (a) Gonzalez, C.; Schlegel, H. B. *J. Phys. Chem.* **1990**, *94*, 5523–5527. (b) Gonzalez, C.; Schlegel, H. B. *J. Chem. Phys.* **1989**, *90*, 2154–2161. (c) Fukui, K. *Acc. Chem. Res.* **1981**, *14*, 363–368.
(12) Frisch, M. J.; et al. *Gaussian 03*, Revision E.01; Gaussian, Inc.: Wallingford, CT, 2004.
(13) Frisch, M. J.; et al. *Gaussian 09*, Revision A.1; Gaussian, Inc.: Wallingford, CT, 2009.
(14) (a) Miertuš, S.; Scrocco, E.; Tomasi, J. *Chem. Phys.* **1981**, *55*, 117–29. (b) Miertuš, S.; Tomasi, J. *Chem. Phys.* **1982**, *65*, 239–45. (c) Pascual-Ahuir, J. L.; Silla, E.; Tuñón, I. *J. Comput. Chem.* **1994**, *15*, 1127–38. (d) Cossi, M.; Barone, V.; Cammi, R.; Tomasi, J. *Chem. Phys. Lett.* **1996**, *255*, 327–35. (e) Cossi, M.; Barone, V.; Mennucci, B.; Tomasi, J. *Chem. Phys. Lett.* **1998**, *286*, 253–60. (f) Cossi, M.; Scalmani, G.; Rega, N.; Barone, V. *J. Chem. Phys.* **2002**, *117*, 43–54.
(15) Siegbahn, P. E. M.; Blomberg, M. R. A.; Chen, S.-L. *J. Chem. Theory Comput.* **2010**, *6*, 2040–2044.
(16) (a) Schwabe, T.; Grimme, S. *Phys. Chem. Chem. Phys.* **2007**, *9*, 3397–3406. (b) Schwabe, T.; Grimme, S. *Acc. Chem. Res.* **2008**, *41*, 569–579.
(17) Karton, A.; Tarnopolsky, A.; Lamère, J.-F.; Schatz, G. C.; Martin, J. M. L. *J. Phys. Chem. A* **2008**, *112*, 12868–12886.
(18) (a) Kutzelnigg, W.; Fleischer, U.; Schindler, M. In *NMR, Basic Principles and Progress*; Diehl, P., Fluck, E., Günther, H., Kosfeld, R., Seelig, J., Eds.; Springer: Berlin, 1991; p 165. (b) Ditchfield, R. *Mol. Phys.* **1974**, *27*, 789. (c) Wolinski, K.; Hilton, J. F.; Pulay, P. *J. Am. Chem. Soc.* **1990**, *112*, 8251.
(19) (a) Douglas, M.; Kroll, N. M. *Ann. Phys. (NY)* **1974**, *82*, 89–155. (b) Hess, B. A. *Phys. Rev. A* **1985**, *32*, 756–63. (c) Hess, B. A. *Phys. Rev. A* **1986**, *33*, 3742–48. (d) Jansen, G.; Hess, B. A. *Phys. Rev. A* **1989**, *39*, 6016–17.
(20) Perdew, J. P.; Burke, K.; Ernzerhof, M. *Phys. Rev. Lett.* **1996**, *77*, 3865.
(21) Pantazis, D. A.; Chen, X.-Y.; Landis, C. R.; Neese, F. *J. Chem. Theory Comput.* **2008**, *4* (6), 908–919.
(22) Weigend, F.; Ahlrichs, R. *Phys. Chem. Chem. Phys.* **2005**, *7*, 3297–3305.
(23) Taken from the freely available ORCA program package. Neese, F. *ORCA-an ab initio, Density Functional and Semiempirical Program Package*, 2.6−35; Universität Bonn: Bonn, Germany, 2008.
(24) (a) Zhao, Y.; Truhlar, D. G. *Theor. Chem. Acc.* **2008**, *120*, 215. (b) Zhao, Y.; Truhlar, D. G. *Acc. Chem. Res.* **2008**, *41*, 157.
(25) Karton, A.; Tarnopolsky, A.; Lamère, J. F.; Schatz, G. C.; Martin, J. M. L. *J. Phys. Chem. A* **2008**, *112*, 12868–12886.
(26) (a) Szalay, P. G.; Bartlett, R. J. *Chem. Phys. Lett.* **1993**, *214*, 481–488. (b) Szalay, P. G.; Bartlett, R. J. *J. Chem. Phys.* **1995**, *103*, 3600–3611. (c) Szalay, P. G. *Chem. Phys.* **2008**, *349*, 121–125.
(27) (a) Jensen, F. *J. Chem. Phys.* **2002**, *117*, 9234. (b) Jensen, F. *J. Chem. Phys.* **2003**, *118*, 2459.
(28) Chong, D. P. *Can. J. Chem.* **1995**, *73*, 79–83.

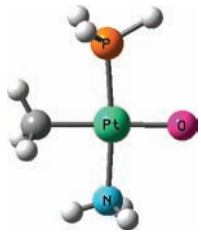

Figure 1. Ball-and-stick representation of the model complex **2M**. Color scheme (used in all figures): C, gray; P, orange; N, blue; O, pink; Pt, green.

etries was analyzed using Natural Bond Orbital (NBO),[29] Mayer bond population analysis,[30] Charge Decomposition Analysis (CDA)[31] and Molecular Orbital Overlap Population (MOOP) analysis.[32] Molden 4.7,[33] GaussView5 and Chemissian[34] software were used for graphic representation of molecular structures and electron densities.

Gaussian was used for all DFT as well as for UMP2 calculations. MOLPRO 2008.1[35] was used for the ROMP2 and CCSD calculations. GIAO−CCSD(T) NMR chemical shift calculations were carried out using the Austin-Mainz-Budapest version of ACES II.[36]

3. Multiplicity State

Since repulsion between occupied Pt orbitals of π symmetry with ligand orbitals of the appropriate symmetry presents the main source of instability of complex **2**, excitation of Pt and/or O valence electrons to higher orbital levels could reduce excess electron density in the bonding area. In support of this, PBE0/PC1 calculations show that there is a triplet state (complex **2t**) 14.8 kcal mol^{-1} below the singlet state of **2** (See Supporting Information for the geometry and electronic structure of **2t**). However, the open shell ground state of the Pt-oxo complex is not consistent with the experimental results, particularly, with NMR spectra of the complex. Changing the functional to M06 and adding of up to 6 diffuse functions on Pt and replacing the basis set on other atoms by pc-2 slightly reduce the singlet−triplet splitting but still show the triplet state of the complex to be lower in energy than the singlet state. On the other hand, it is pretty well-known that hybrid density functional methods are biased in favor of high-spin states. To shed light on the issue, we first compared performance of DFT and *ab initio* methods for the small model system $(PH_3)(NH_3)(CH_3)Pt{=}O$ (complex **2M**, Figure 1). Similarly to complex **2**, complex **2M** is more stable in the triplet state according to DFT (PBE and PBE0) calculations, but is more stable in the singlet state according to MP2 calculations (Table 1). As MP2 method generally favors low-spin states, these results do not allow to decide unambiguously on the ground state of the model complex.

Table 1. Singlet−Triplet Splitting ($E_{triplet} - E_{singlet}$, kcal mol^{-1}) in the Model Complex **2M** Calculated Using DFT and MP2 Methods Combined with Different Polarization Consistent Basis Sets

	PC1	AUG-PC1	PC2	AUG-PC2
PBE0	−10.06	−8.87	−8.74	−8.84
PBE	−4.91	−2.97	−2.75	−2.87
UMP2	16.64	17.86	19.13	19.04

Table 2. Singlet−Triplet Splitting ($E_{triplet} - E_{singlet}$, kcal mol^{-1}) in the Model Complex **2M** Calculated Using Different *ab initio* and Double Hybrid B2GP-BLYP Methods

	spd/vdz	spd/vtz	spdf/vtz	spdf/avtz
HF	−31.11	−30.45	−29.40	−29.14
ROMP2	7.02	8.73	10.41	11.30
CCSD	−9.70	−8.19	−6.89	−5.94
CCSD[T]	−4.88	−2.96	−1.60	−0.50
CCSD(T)	−5.16	−3.22	−1.84	−0.76
B2GP-BLYP	−2.79	−0.62	0.23	0.71

Systematic *ab initio* calculations on complex **2M** show strong dependence of the singlet−triplet splitting on the electron correlation level (Table 2). At the most accurate CCSD(T) level the triplet state is only a few kcal mol^{-1} more stable than the singlet state. Expanding the basis set favors the closed shell state of the complex. Thus, the singlet and triplet complexes **2M** are virtually isoenergetic with the largest basis set used. To rule out the possibility of a low-lying open-shell singlet state, we carried out AQCC calculations in the smallest basis set on the singlet and the triplet states, as well as on the open-shell singlet state at the triplet geometry. At the AQCC level, we found the singlet on the bottom, the triplet at 8.17 kcal/mol above, and the OSS at 28.46 kcal/mol above. Thus, the open-shell singlet was eliminated from further consideration.

The recently published double hybrid B2GP-PLYP functional,[40] which is capable of accurately treating Rydberg-type orbitals,[41] provides reasonable agreement with the CCSD(T) benchmark. This method was applied for calculation of the singlet−triplet splitting in complex **2**. Our B2GP-PLYP results show the open-shell state of complex **2** to be more stable than the closed-shell state by 4.33, 2.76, and 1.80 kcal mol^{-1} when the basis set is increased from spd/vdz to spd/vtz and to spdf/vtz. One could suggest that at the basis set limit of the B2GP-PLYP method the singlet and triplet states of complex **2** are equally stable. Coordination of a solvent molecule further stabilizes the singlet state (see below) thus leading to the diamagnetic Pt oxo complex observed experimentally.

4. Interactions with Solvent and Ancillary Ligands

In search of the factors that stabilize complex **2** in acetone solution we considered its interactions with BF_4^- counterion, with solvent molecules and with water molecules, presence of

(29) Reed, A. E.; Curtiss, L. A.; Weinhold, F. *Chem. Rev.* **1988**, *88*, 899–926.
(30) (a) Mayer, I. *Chem. Phys. Lett.* **2000**, *332*, 381. (b) Mayer, I.; Hamza, A. *Program "APOST*, Version 1.07; Chemical Research Center, Hungarian Academy of Sciences: Budapest, 2000−2004.
(31) Dapprich, S.; Frenking, G. *J. Phys. Chem.* **1995**, *99*, 9352–9362.
(32) (a) Hoffmann, R. *Solids and Surfaces: A Chemist's View of Bonding in Extended Structures*; VCH: Weinheim, 1988; pp 42−55. (b) *GaussSum 1.0*; O'Boyle, N. M., Ed.; Dublin City University: Dublin, Ireland, 2005. Available at http://gausssum.sourceforge.net.
(33) Schaftenaar, G.; Noordik, J. H. *J. Comput.-Aided Mol. Design* **2000**, *14*, 123–134.
(34) Available from http://www.chemissian.com.
(35) Werner, H.-J.; et al. *MOLPRO, a package of ab initio programs*, version 2008.1; 2008;http://www.molpro.net.
(36) Stanton J. F.; Gauss J.; Watts J. D. et al. ACES II, Austin-Mainz-Budapest version; See also http://www.aces2.de.
(37) Calculations were performed using Gaussian 03. See the Computational Methods section for details.
(38) Deviation in the MP2 data in Tables 1 and 2 should be attributed to different computational methods (UMP2 and ROMP2, respectively) and to larger spin contamination in the former (>0.04) than in the latter (0.004−0.005) case.
(39) All *ab initio* calculations were carried out using MOLPRO2008.1. B2GP-BLYP calculations were carried out using Gaussian 03. See the Computational Methods section for details.
(40) Karton, A.; Tarnopolsky, A.; Lamère, J. F.; Schatz, G. C.; Martin, J. M. L. *J. Phys. Chem. A* **2008**, *112*, 12868.
(41) Goerigk, L.; Moellmann, J.; Grimme, S. *Phys. Chem. Chem. Phys.* **2009**, *11*, 4611–4620.

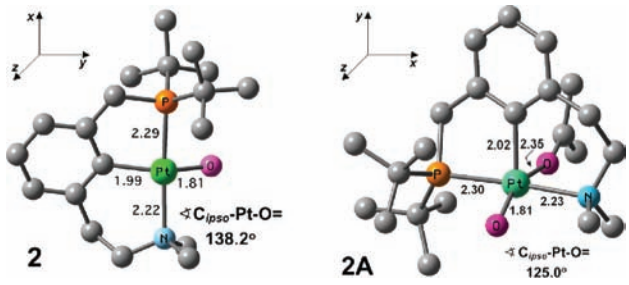

Figure 2. Optimized geometries of the Pt-oxo complex without an ancillary ligand (**2**) and with coordinated acetone molecule (**2A**). Hydrogen atoms are omitted for clarity.

which in trace amount could not be completely excluded at the experimental conditions. Moreover, taking into account the highly polar nature of Pt-oxo bond, we also considered possible protonation of complex **2**.

In our previous publication,[5] we reported that acetone, water, and BF_4^- coordination to complex **2** are thermodynamically unfavorable. However, because of the small energy values, qualitatively different results were obtained using a more accurate approach applied in the present work. At our present theoretical level coordination of all three ligands is thermodynamically favorable with ΔG^0_{298} of −3.18, −0.07, and −4.59 kcal mol^{-1} for acetone, water and BF_4^-, respectively. The ΔG^0 values obtained from quantum chemical calculations relate to the standard state of one molar concentration of the reagents. In order to judge about the most stable form of complex **2** and its stability in solution, the chemical potential of the ligands should be taken into account. Thus, the high concentration of the acetone ligand in acetone solution (13.645 mol l^{-1}) leads to the effective $\Delta G_{298} = \Delta G^0_{298} - RT \ln C_{\text{acetone}} = -4.73$ kcal mol^{-1} while low concentration of BF_4^- (0.015 mol l^{-1}) results in the effective $\Delta G_{298} = -2.10$ kcal mol^{-1}. These values are used in the further discussion as Gibbs free energies of the corresponding complexes in acetone solution. We did not find complex **2t** with coordinated acetone or water molecule, since Pt-acetone and Pt-water interactions have mostly repulsive character in the triplet state; thus, the corresponding bonds were broken during geometry optimization. Coordination of BF_4^- anion to **2t** is pronouncedly more endergonic (ΔG_{298}=+2.10 kcal mol^{-1}) than its coordination to **2**. Thus, comparison of ΔG values for the three ligands unambiguously shows that **2** contains a coordinated solvent molecule in acetone solution (complex **2A**). Taking into account the B2GP-PLYP results on the singlet−triplet splitting presented above, this complex is at least 2.93 kcal mol^{-1} more stable than the most stable triplet state.

The optimized geometry of **2A** with coordinated acetone molecule in comparison with the "bare" complex **2** is shown in Figure 2. The nature of the Pt-acetone interaction is noticeably ionic, with a Pt−O bond length of 2.35 Å and a Wiberg bond index (WBI) of 0.23. Formation of the Pt···OC(CH$_3$)$_2$ bond is accompanied by acetone → Pt charge transfer of 0.19 electron, according to NBO analysis. This excess of electron density causes elongation of Pt−N, Pt−P and Pt−C$_{ipso}$ bonds (Figure 2), while Pt-oxo bond remains nearly untouched. Stabilization of the Pt-oxo bond is achieved by further bending of the Pt-oxo bond out of the plane of the complex (∠C$_{ipso}$−Pt−O decreases from 138.2° in **2** to 125.0° in **2A**), so that the geometry of complex **2A** is closer to a distorted trigonal bipyramid than to a square pyramid.

Activation of a C−H bond of the acetone ligand in **2A** with formation of a hydroxo complex is thermodynamically favorable, but is not accessible kinetically (see Supporting Information). Attempts to optimize the geometry of the Pt-oxo complex with two coordinated acetone molecules brought about breaking of one of the metal−ligand bonds or led to strongly endergonic hydrogen transfer from one of the ligands to oxo oxygen.

Protonation presents another common kind of interaction between electron-rich transition metal complexes and a solvent. Our results indicate that protonation of complex **2** in acidic media is thermodynamically favorable while proton abstraction from water is strongly unfavorable (see Supporting Information). However, when the resulting OH^- anion is coordinated to the complex, the energetic results are completely different. This interaction is in fact the reaction of water activation and it will be discussed below.

Summarizing, our present results indicate that complex **2** adopts form **2A** with one weakly coordinated solvent molecule in acetone solution. That provides additional stabilization of the singlet state of the complex with respect to the open shell state. Chemical transformations of the coordinated acetone molecule, as well as coordination of other ancillary ligands presented in the reaction mixture could be excluded based on thermodynamic or kinetic considerations. Protonation of the Pt-oxo group does not occur in the nonacidic media described in ref[5] but could be highly expected for intermediate catalytic oxo complexes in the presence of proton donors.

5. Calculated NMR

The NMR chemical shifts can be used to identify the disposition of valence electrons in a molecule. All the complexes presented in our previous publication[5] were characterized by NMR. Hence, theoretical NMR analysis allows us to better understand the electronic structure of the complexes while similarity with the experimentally obtained spectra provides a strong link between the experimentally obtained complexes and their calculated structures. Herein we compare the ^{13}C, ^{1}H and ^{195}Pt chemical shifts calculated for complexes **1**, **2**, **3** and **4** with the corresponding experimental results.

a. ^{13}C and ^{1}H NMR. Extensive literature sources have demonstrated that GIAO DFT calculations can be an asset in interpreting of NMR spectra.[42] Accuracy of the predicted chemical shifts strongly depends on the applied theoretical method. Particularly, good geometry and large augmented basis set to be applied in such calculations were especially stressed. Correct prediction of ^{13}C and ^{1}H chemical shifts could be now routinely achieved for small- and medium-sized organic molecules. However, the presence of transition metal atoms in a molecule lowers the reliability of the predicted ^{13}C and ^{1}H NMR spectra because of the lower theoretical level applied in such calculations. Moreover, as far as heavy atoms are to a large extent influenced by relativistic effects, they may induce spin−orbit shielding in neighboring light nuclei known as "heavy-atom effect on the light atom shielding".[42c,43] This effect is not accounted for by the spin-free relativistic approximations

(42) (a) Dybiec, K.; Gryff-Keller, A. *Magn. Reson. Chem.* **2009**, *47*, 63–66, and references herein. (b) Bagno, A. *Chem.−Eur. J.* **2001**, *7*, 1652–1661. (c) Bagno, A.; Saielli, G. *Theor. Chem. Acc.* **2007**, *117*, 603–619. (d) Schreckenbach, G.; Ziegler, T. *Theor. Chem. Acc.* **1998**, *99*, 71–82.

(43) (a) Fukui, H.; Baba, T. *J. Chem. Phys.* **2002**, *117*, 7836–7844. (b) Kaupp, M.; Malkina, O. L.; Malkin, V. G.; Pyykko, P. *Chem.−Eur. J.* **1998**, *4*, 118. (c) Morishama, I.; Endo, K.; Yonezawa, T. *J. Chem. Phys.* **1973**, *59*, 3356. (d) Kaupp, M.; Malkina, O. L.; Malkin, V. G.; Pyykkö, P. *Chem.−Eur. J.* **1998**, *4*, 118–126.

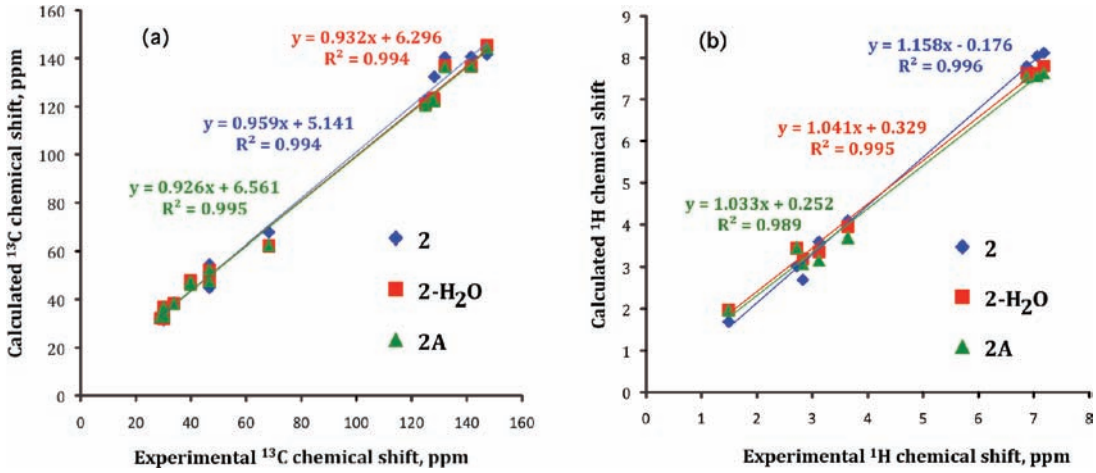

Figure 3. Calculated versus experimental (a) ^{13}C and (b) ^{1}H chemical shifts in Pt-oxo complex without ancillary ligands (**2**) and with coordinated water (**2-H_2O**) or acetone (**2A**) molecule. Calculated shifts for chemically equivalent protons in methyl and methylene groups are averaged. The shifts are calculated at the PBE0/PC-1 level of theory and scaled with respect to the *ab initio* chemical shifts of small nonpolar molecules (see Supporting Information for details).

applied in the present work (relativistic ECP on Pt and all-electron scalar relativistic second-order DKH approach). The presence of a solvent adds complexity to the theoretical prediction of NMR spectra, especially when it forms additional localized bonds (e.g., hydrogen bonds) with the molecule of interest. Thus, we expect qualitative rather than quantitative agreement of the theoretical NMR data obtained in the present work with the corresponding experimental observation.

Typical dependencies of predicted versus experimental ^{13}C and ^{1}H chemical shifts in complex **2** are shown in Figure 3. Qualitatively, all three approaches described in Computational methods reproduce well the experimentally observed ^{13}C and ^{1}H NMR spectra. Quantitatively, calculations at the PBE0/PC-1 level of theory and scaling with respect to *ab initio* chemical shifts give somewhat superior results for ^{13}C chemical shielding. For complex **2A** it yields the largest deviation of calculated δ_C from the experimental data of 8.0 ppm, a reasonable error that could be attributed to the neglected spin−orbit coupling.[44] For ^{1}H NMR this approach is slightly worse than nonrelativistic and relativistic results scaled with respect to experimental data ($\Delta\delta_H$ is 3.3, 1.0, and 1.2 ppm for averaged PC(CH_3) while for other H atoms $\Delta\delta_H$ does not exceed 3.0, 0.8, and 0.5 ppm, respectively).[45]

The most interesting feature of the ^{13}C chemical shift was observed for the C_{ipso} atom in complex **2**. Indeed, one would expect that oxidation of Pt(II) to Pt(IV) (reaction 1 in Scheme 2) should result in a decrease of electron density on this atom, and thus deshielding. However, the opposite is observed: an upfield chemical shift from 150.61[46] to 147.25 ppm was found for C_{ipso} experimentally, while the calculated chemical shifts with the three computational methods applied change from 144.3−150.2 to 141.6−148.7 ppm for **1** → **2** and from 149.4−155.2 to 144.4−149.2 ppm for **1A** → **2A**. This finding should be attributed to a repulsive interaction with the electron rich oxo ligand (see below). The electronic structure analysis demonstrates that, as expected, the total electron density on the C_{ipso} strongly decreases upon oxidation (NBO charges are −0.173 in **1A** and −0.118 in **2A**); however, this is due to depopulation of the valence 2p and diffuse 3s, 3p orbitals (total by 0.371 electron) while populations of the compact 1s and 2s orbitals *increase* by 0.004 and 0.012, respectively, so that electron density in close proximity of the C_{ipso} nucleus is higher in **2A** than in **1A**.

Acetone coordination in complex **2A** causes a downfield shift of 13.5−19.1 ppm for the ketonic C, too small to be detected in presence of acetone solvent, while average ^{13}C and ^{1}H shifts of the methyl groups are virtually untouched. Very similar results were obtained for complexes **1A** and **3A**.

Concluding, calculated and experimental ^{13}C and ^{1}H NMR spectra show close similarity, thus confirming the atomic structure of the synthesized complex **2**. These calculations helped us in the assignment of observed NMR peaks in complexes with complicated structures (see Supporting Information). However, in general, the ^{13}C and ^{1}H chemical shifts of identical groups in complexes **1**, **2**, **3** and **4** are found in close proximity, both experimentally and theoretically. Likewise, calculated ^{13}C and ^{1}H NMR spectra show only minor dependence on the presence of ancillary ligands. Therefore, these data provide limited insight into the structure and composition of the complexes in hand. Calculated and experimental ^{31}P chemical shifts show very similar behavior and thus are not discussed here.

b. ^{195}Pt NMR. In contrast, the ^{195}Pt chemical shift, which varies in an extremely wide range,[47] is a very sensitive probe to examine the oxidation state and ligand environment of platinum complexes. It was shown that the PBE density functional performs quite well for Pt chemical shifts[48] while hybrid functionals perform somewhat better.[49] However, even

(44) Wolff, S. K.; Ziegler, T. *J. Chem. Phys.* **1998**, *109*, 895–905.
(45) The relatively low accuracy of ^{1}H NMR arises from its strong sensitivity to formation of hydrogen bonds with solvent molecules that are not properly accounted for by the continuum solvation model applied in the present work. Even worse results obtained for averaged PC(CH_3) protons should be partially attributed to formation of weak Pt···H agostic bonds that slow down free rotation of the CH_3 and C(CH_3) groups and make the protons not completely equivalent.
(46) Poverenov, E.; Gandelman, M.; Shimon, L. J. W.; Rozenberg, H.; Ben-David, Y.; Milstein, D. *Organometallics* **2005**, *24*, 1082–1090.
(47) Juranic, N. *Coord. Chem. Rev.* **1989**, *96*, 253–290, and references herein.
(48) (a) Fowe, E. P.; Belser, P.; Daul, C.; Chermette, H. *Phys. Chem. Chem. Phys.* **2005**, *7*, 1732. (b) Koch, K. R.; Burger, M. R.; Kramer, J.; Westra, A. N. *Dalton Trans.* **2006**, 3277. (c) Sterzel, M.; Autschbach, J. *Inorg. Chem.* **2006**, *45*, 3316.
(49) Autschbach, J.; Zheng, S. *Magn. Reson. Chem.* **2006**, *44*, 989.

Table 3. ^{195}Pt Chemical Shifts[a] and NBO Charges on Pt Atom[b] in PCN−Pt Complexes

	^{195}Pt chemical shift			
	PBE/PC1	PBE0/PC1	experimental	NBO charge on Pt
1	−4094.54	−4338.37	−4015.00	0.182
1A	−4147.73	−4473.30		0.165
2	1395.17	1521.50		0.517
2A	−905.36	−791.98	−645.88	0.494
2-H_2O	−1050.02	−949.94		0.936
3	−2763.03	−3025.93	−2842.87	0.587
3A	−2496.38	−2853.86		0.445
***trans*-4**	−1684.44	−1484.88		1.028
***trans*-4-(H_2O)**	−1427.28	−1188.05		1.051
***trans*-4-(H_2O)$_2$**	−1454.22	−1220.46	−524.03	1.047
***trans*-4-(H_2O)$_2$-a**	−1320.55	−1058.06		1.053
***trans*-4-(H_2O)$_3$**	−1294.56	−1035.87		1.054

[a] Calculated using PBE and PBE0 density functionals combined with SARC-DKH basis set on Pt and TZV-DKH basis set on others elements. [b] Calculated using PBE0/PC1 combination.

though special methods and programs for the calculation of NMR properties are available and relativistic effects are properly accounted for, calculations of platinum chemical shifts are not straightforward because they are very sensitive to the geometry of the complex and to solvent and thermal effects.[50] In this work we applied PBE and PBE0 functionals, including relativistic effects, by means of the two-component DKH approximation with bulk solvent effect, accounted for by a continuum (IEF-PCM) model and partially by explicit inclusion of solvent molecules. The obtained ^{195}Pt chemical shifts for complexes **1**, **2**, **3** and *trans*-**4** in absence and presence of ancillary ligands are shown in Table 3.

It could be seen from Table 3 that both pure and hybrid functionals bring about qualitatively similar results. Calculated ^{195}Pt chemical shifts in complexes **1** and **3** are in satisfactory agreement with the corresponding experimental data. Acetone coordination in complex **1** causes a relatively small (by 58 and 135 ppm, respectively, using PBE and PBE0 functionals) upfield shift of the ^{195}Pt NMR signal that, according to the calculated NBO charges, could be directly attributed to an electron donation from the ligand. Acetone coordination in complex **3** causes a downfield shift of the signal (by 289 and 172 ppm, respectively) accompanied by a decrease of the positive charge on the Pt atom, indicating redistribution of the electron density from compact to more diffuse Pt atomic orbitals.

In contrast, the calculated ^{195}Pt chemical shift in complex **2** significantly differs from the measured one. However, acetone or water coordination results in a dramatic (by 2313−2691 ppm) upfield shift so that ^{195}Pt chemical shift in **2A** becomes well consistent with the experimental data. The stronger electron donating water ligand causes an even larger deshielding of the Pt nucleus so that the calculated ^{195}Pt chemical shift in **2-H_2O** is notably more negative than the measured one. These results, together with the thermodynamic stabilities of complex **2** in the presence of ancillary ligands discussed above, confirm our conclusion that complex **2** adopts the form **2A** in acetone solution at room temperature. A similar strong effect of the ancillary ligands was found in recent relativistic DFT calculations of ^{195}Pt NMR chemical shift in complexes **2**, **2A** and **2-H_2O**.[51] The Becke-88 exchange plus the Perdew-86 correlation functional with basis sets of double- and triple-ζ quality and relativistic effects accounted for by ZORA approximation were applied in that work. The ^{195}Pt NMR signal of complex **2** was found in that approach at 3808.76 ppm while acetone, water and pyridine ligands change this value to 149.41, −388.61, and −747.50 ppm, respectively, thus also indicating that an ancillary ligand is coordinated with complex **2** in acetone solution. However, in contrast to our calculations, these results show that water and, especially, pyridine ligands bring about better agreement with the experiment than acetone.

The ^{195}Pt NMR signal in complex *trans*-**4** is calculated to be at a much higher field than found experimentally (Table 3). In contrast to complexes **1**, **2** and **3**, which were obtained and characterized in organic (acetone) solvent, complex **4** was synthesized in the presence of a large excess of water. Autschbach and co-workers have shown that deviations of up to several thousand ppm between calculated and experimental ^{195}Pt chemical shifts are due to the solvent effect. Indeed, explicit inclusion of the first second-sphere water molecule (complex *trans*-**4-(H_2O)**) shifts the signal downfield by 278 (PBE) /297 (PBE0) ppm. However, further addition of second-sphere water molecules bound by hydrogen bonds to the first-sphere OH and water ligands causes much smaller changes in the calculated NMR spectrum. The optimized geometries of *trans*-**4** without and with up to three second-sphere water molecules are shown in Figure 4. One can see that the first second-sphere water molecule causes the strongest changes in the first coordination sphere of the complex. Additional water molecules have a much smaller geometric effect. Moreover, the positions of these molecules significantly influence both the geometry of the complex and the calculated ^{195}Pt chemical shift. Comparing the calculated solvated complexes with the experimentally observed X-ray structure of complex **4** (Figure 4) shows that many more water molecules are coordinated around the complex even in solid state. That clearly demonstrates that explicit modeling of complex *trans*-**4** in water-acetone media is hardly possible. Moreover, supermolecule Pt NMR calculations on static complexes are not sufficient because of neglecting of dynamic effects.[50] Currently the most appropriate approximation is DFT-based molecular dynamics simulations.[50d] Such calculations were recently performed on small Pt complexes.[50c] We believe that accurate treatment of the solvent cavity will further improve the obtained values; however, detailed study of the solvent effect on complex **4** was beyond the scope of the present work.

It is interesting to note that the downfield shift of the calculated ^{195}Pt NMR signal, in general, linearly correlates with increasing positive charge on Pt atom (Figure 5), indicating deshielding of the Pt nucleus in more oxidized states. Two of the calculated complexes, **2** and **2A**, break the trend. The much lower-field chemical shift in these complexes than is determined by the total positive charge indicates their specific electronic structure. This important feature will be analyzed below.

6. Reactivity of Pt-Oxo Complex

Experimentally it was found that complex **2** shows diverse reactivity.[5] The aim of this part is to get deeper insight into the

(50) (a) Pregosin, P. S. *Coord. Chem. Rev.* **1982**, *44*, 247–291. (b) Sterzel, M.; Autschbach, J. *Inorg. Chem.* **2006**, *45*, 3316–3324. (c) Truflandier, L. A.; Autschbach, J. *J. Am. Chem. Soc.* **2010**, *132*, 3472–3483. (d) Vaara, J. *Phys. Chem. Chem. Phys.* **2007**, *9*, 5399–5418. (e) Gilbert, T. M.; Ziegler, T. *J. Phys. Chem. A* **1999**, *103*, 7535. (f) Sterzel, M.; Autschbach, J. *Inorg. Chem.* **2006**, *45*, 3316. (g) Sterzel, M.; Autschbach, J. *Inorg. Chem.* **2006**, *45*, 3316–3324.

(51) Bagno, A.; Bini, R. *Angew. Chem., Int. Ed.* **2009**, *49*, 1083–1086.

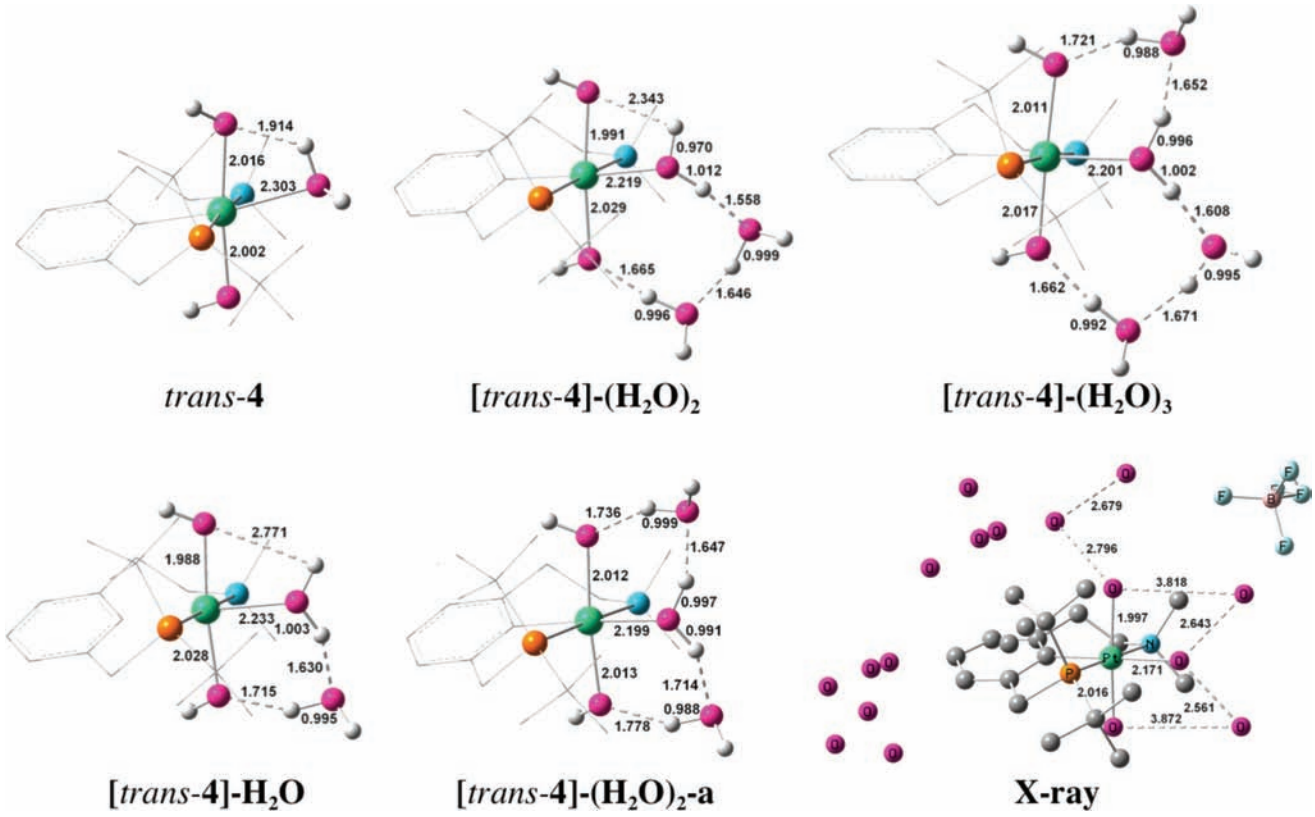

Figure 4. Optimized geometries of *trans*-**4** with 0, 1, 2, and 3 s-sphere water molecules in comparison with the experimentally observed X-ray structure of **4**.

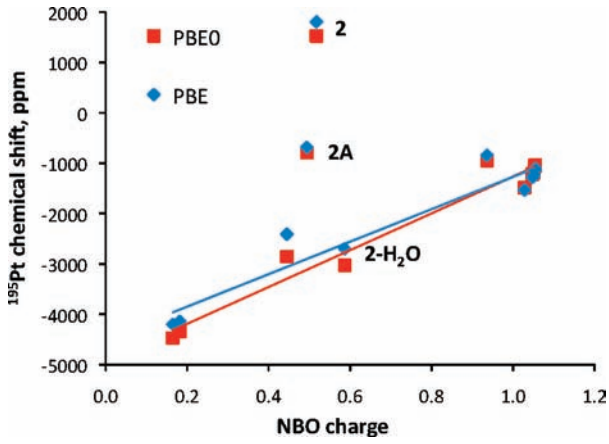

Figure 5. Correlation between NBO charge on Pt atom and calculated ^{195}Pt NMR chemical shift in PCN−Pt complexes listed in Table 3.

reactivity of the terminal Pt oxo complex from the mechanistic viewpoint. We focus on the mechanisms of intramolecular oxygen transfer, of CO and hydrogen oxidations and of water activation (reactions 3−6 in Scheme 2). For all interactions, both the reactivity of complex **2** in presence of an ancillary acetone ligand (complex **2A**), and with its prior dissociation, are addressed. Unless stated otherwise, energetic results presented herein are Gibbs free energies in acetone solution (ΔG_{298}) referred to complex **2A**.

a. Intramolecular Oxygen Transfer. Second order perturbation theory analysis of Fock matrix of complex **2** in NBO basis shows that stabilization gained by π-type conjugative delocalization from the partially populated Pt $6p_z$ lone pair to σ^* Pt−C_{ipso} orbital is extremely powerful. However, Pt−C_{ipso} bond breaking is prevented by the structure of the pincer PCN ligand. Delocalization from the Pt $6p_z$ lone pair to σ^* Pt−P orbital presents the next strong electron excitation. Experimentally, this interaction manifests itself in intramolecular oxygen transfer, resulting in insertion of the oxo ligand into the Pt−P bond to give complex **3** (reaction 3 in Scheme 2). This transformation is accompanied by an energy gain of 62.22 kcal mol^{-1} with a small activation barrier of 7.66 kcal mol^{-1} (Scheme 3). However, geometry optimization of the transition state for **2A** → **3A** transition demonstrated that complex **2A** bearing a coordinated solvent molecule does not undergo such interaction, and dissociation of the ancillary ligand precedes the reaction. It results in an apparent activation barrier of 12.38 kcal mol^{-1}, in reasonable agreement with the experimentally observed moderate stability of complex **2**.

b. CO Oxidation. Carbon monoxide oxidation by Pt oxo complexes **2** and **2A** yielding, respectively, three-coordinated (**1**) and solvated (**1A**) products are thermodynamically strongly favorable (Scheme 4). Reaction profiles for these interactions are shown in Figure 6. We found two isomeric carbonyl Pt oxo complexes, *trans*-**5** and *cis*-**5**. The geometry of *trans*-**5** is close to distorted trigonal bipyramid with ∠C_{ipso}−Pt−O = 129.2° and CO effectively *trans* to oxo O (∠OC−Pt−O = 158.4°). Similar configurations were found for the solvated five-coordinated Pt oxo complexes, as discussed above. However, the fact that CO is not only a σ donor, but also a powerful π acceptor, results in strong Pt-CO bonding ($WBI_{Pt\text{-}CO}$ = 0.68). According to NBO analysis, there is 0.49 electron transfer in the σ direction and 0.38 electron π backdonation in *trans*-**5**. On the other hand, the CO ligand dramatically weakens both Pt−O and Pt−C_{ipso} bonds (WBI_{Pt-O} reduces from 1.31 in **2** to 0.78 in *trans*-**5** and WBI reduces from 0.78 to 0.51). For comparison, acetone

Scheme 3. Mechanism of Intramolecular Oxygen Transfer in Complex **2A**[a]

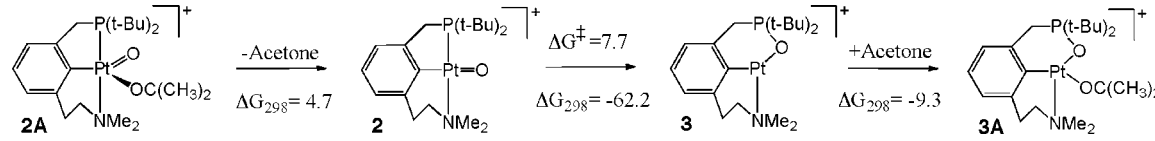

[a] Reaction energies and activation barrier (in kcal mol^{-1}) in acetone solution are given for each step. For the overall transformation $\Delta G_{298} = -66.8$ kcal mol^{-1}.

Scheme 4. Overall Reaction Energies (in kcal mol^{-1}) of CO Oxidation by Complexes **2** and **2A** in Acetone Solution

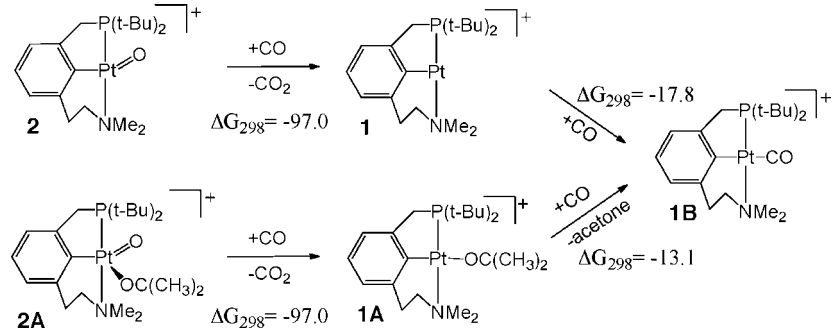

coordination in **2A** results in $WBI_{Pt-O} = 1.29$ and WBI = 0.72). Consequently, *trans*-**5** is only moderately stable with respect to individual **2** and CO ($\Delta G_{298} = -16.15$ kcal mol^{-1}).

The second isomer, *cis*-**5**, has a slightly distorted square pyramidal configuration with oxo O in the axial position and CO *trans* to C_{ipso}. This complex is characterized by much smaller electron transfer (0.33 e$^-$ in the CO → Pt direction and 0.18 e$^-$ backdonation) and a much weaker Pt-CO bond (WBI_{Pt-CO} = 0.47). Thus, destabilization of Pt bonding with the oxo and aryl ligands is smaller (WBI_{Pt-O} = 0.85 and WBI=0.54) and, in consequence, stability of complex *cis*-**5** is high (ΔG_{298}=−32.68 kcal mol^{-1} with respect to the individual reagents).

On geometric grounds, interaction between the CO and oxo O ligands is possible only in the *cis* isomer. In the transition state **TS(5−1)** both ligands are bent from their equilibrium positions so that ∠O−Pt−CO changes from 83.9° in *cis*-**5** to 66.4°. The corresponding weakness of the Pt-CO bond (WBI_{Pt-CO} = 0.41 with respect to 0.47 in *cis*-**5**), which is not accompanied by strengthening of other bonds, is responsible for the calculated activation barrier of 37.85 kcal mol^{-1}, too high for a room temperature reaction.

Unlike other ligands considered, CO interaction with **2A** to give the six-coordinated complex **5A** (see Figure 6) is exoenergetic ($\Delta H < 0$), although entropy and solvation effects make the formation of **5A** endergonic at room temperature (ΔG_{298} = +6.90 kcal mol^{-1}). Complex **5A** has an octahedral configuration with the CO ligand located in the plane of the PCN ligand while the oxo O and acetone ligands are found in the axial positions. Formation of **5A** from electron rich complex **2A** is possible because of the π-acceptor ability of the CO ligand, that allows

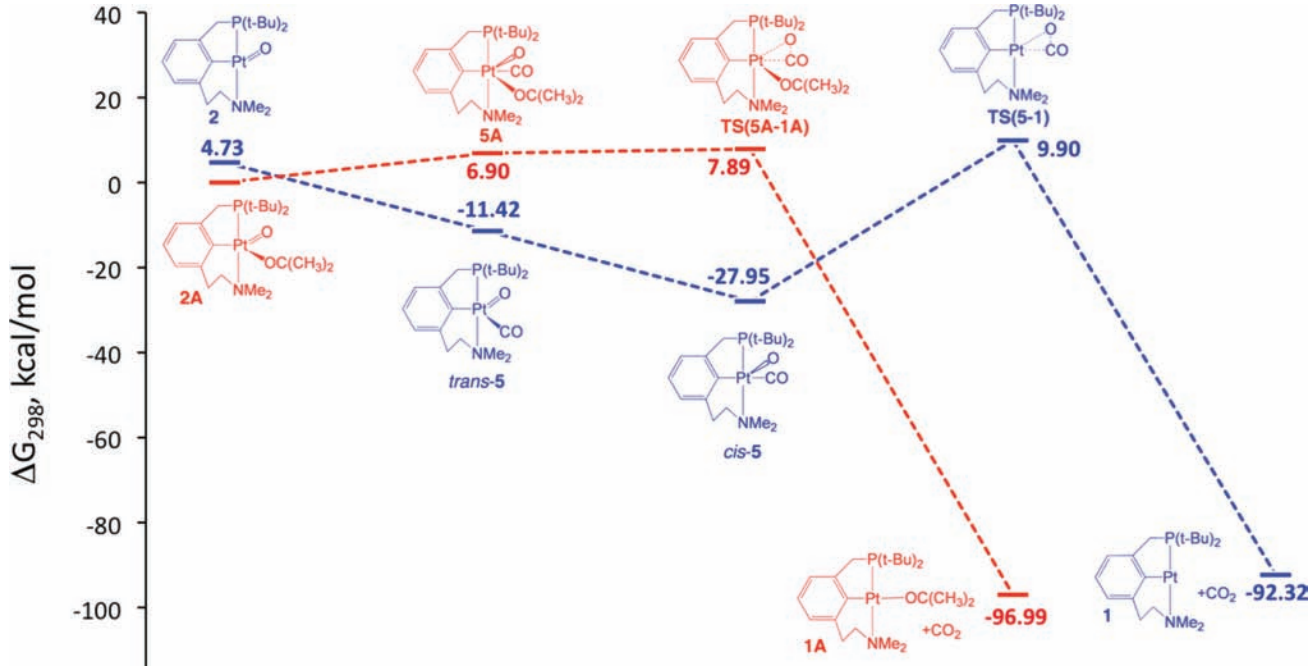

Figure 6. Reaction profiles for CO oxidations by Pt oxo complexes **2** (blue) and **2A** (red). All the complexes retain positive charge +1.

Scheme 5. Overall Reaction Energy (in kcal mol^{-1}) for H_2 Oxidation by Complex **2A** in Acetone Solution

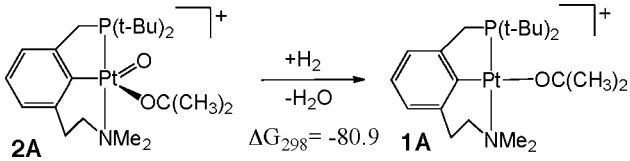

for partial relief of excess electron density on the metal atom. Indeed, although the total natural charge on the coordinated CO in **5A** is +0.14, it presents the result of CO → Pt σ donation of 0.33 e$^-$ and Pt → CO π backdonation of 0.20 e$^-$. These electronic transitions result in quite strong Pt-CO bonding (WBI_{Pt-CO} = 0.43) at the expense of the Pt−O bond (WBI_{Pt-O} decreases from 1.29 in **2A** to 0.51 in **5A**) while Pt−C_{ipso} bond slightly strengthens upon CO coordination (WBI increases from 0.72 to 0.76, respectively). Destabilization of the Pt−O bond and relatively low stability of the carbonyl complex **5A** make CO oxidation easy. The interaction proceeds through an early transition state **TS(5A−1A)** (see Figure 6), in which ∠O−Pt−CO = 68.9° (in comparison with 76.5° in **5A**), with a calculated apparent activation barrier $\Delta G^{\ddagger}_{298}$ = 7.89 kcal mol^{-1}. Therefore, the acetone ligand in the coordination sphere of the Pt oxo complex facilitates CO oxidation mostly by destabilization of the initial carbonyl complex.

c. Hydrogen Oxidation. Hydrogen oxidation by the Pt oxo complex (reaction 5 in Scheme 2) is strongly exergonic (Scheme 5). Experimentally, reaction 5 is completed within 12 h at room temperature with 52% yield and complex **3** being a competitive product. The calculated reaction profile for H_2 oxidation by the Pt oxo complex is shown in Figure 7. Similar to CO coordination, hydrogen activation by transition metal complexes also involves electron donation from the occupied H_2 σ orbital and backdonation from the metal atom to the σ* orbital of H_2. Nonetheless, hydrogen shows much poorer electron withdrawing ability than CO because of higher energy of its lowest empty orbital. Hence, hydrogen interaction with the pentacoordinated complex **2A** is repulsive, and acetone dissociation presents a mandatory first step in reaction (5). Hydrogen interaction with the resulting complex **2** is attractive, although formation of the σ complex **6** (see Figure 7) is slightly endergonic in acetone solution at room temperature (ΔG_{298}=+5.67 kcal mol^{-1}). The H_2→Pt electron donation of 0.34 e$^-$ and backdonation of 0.08 e$^-$ to the σ* orbital of H_2 result in ∠C_{ipso}−Pt−O = 122.4° in **6**. The activated hydrogen molecule in this complex is situated virtually *trans* to the terminal oxo ligand while ∠C_{ipso}−Pt−H is only 63.9°. The oxo ligand in complex **6** shows higher affinity to the phosphine ligand than in complex **2** thus opening a low-energy reaction channel toward the competitive product **3**. In particular, ∠P−Pt−O decreases from 89.9° in **2** to 87.5° in **6**, and WBI_{P-O} increases from 0.079 to 0.109.

High electron density on the Pt atom encourages backdonation to the σ* orbital of the coordinated H_2, so that the transition state for hydrogen dissociation **TS(6−7)** is virtually isergonic with **6** on the ΔG_{298} PES. Increased Pt→H_2 backdonation causes H−H bond elongation from 0.851 Å in **6** to 0.996 Å in **TS(6−7)**. Diminished electron density on Pt due to backdonation, in turn, results in relief of the oxo O bending out of the plane of the complex (∠C_{ipso}−Pt−O = 135.2° in **TS(6−7)** in comparison with 122.4° in **6** and 138.2° in **2**).

By virtue of the fact that complex **2** disfavors oxidative addition of σ donor ligands, we did not locate a dihydrido complex on the PES. Following the intrinsic reaction coordinate, we found that **TS(6−7)** directly leads to agostic hydrido complex **7** (Figure 7), in which one of the hydrogens is bound to both Pt and C_{ipso} atoms. Formation of **7** is exergonic by 6.30 kcal mol^{-1} with respect to individual **2** and H_2. The agostic interaction significantly changes the geometric and electronic structures of the complex. Particularly, the Pt−C_{ipso} bond is nearly broken; its length increases from 1.99 Å in **2** to 2.40 Å in **7** (Figure 8), and WBI decreases from 0.78 to 0.15. The aromatic ring is bent out of the plane of complex **7**, forming a dihedral angle of 121.1° with Pt. Thus, the firm Pt−C_{ipso} σ bonding, accompanied by strong repulsion between occupied aromatic π orbitals and Pt 5d orbitals of the appropriate symmetry in **2**, is replaced by weak interaction between Pt and C_{ipso} p_π orbitals in **7**. This results in diminished Pt−O π repulsion, followed by further relief of the oxo O bending with respect to the plane of the complex (∠C_{ipso}−Pt−O = 153.8° in comparison with 122.4° and 135.2° in **6** and **TS(6−7)**, respectively).

Migration of the hydride H to oxo O to give agostic hydroxo complex **8** is the following step on the reaction pathway. The transition state for this migration, **TS(7−8)** in Figure 7, is characterized by a decrease of the H−Pt−O bond angle to 66.5° (in comparison with 119.5° in **7**). This quite strong angular transformation leads to a local activation barrier as small as 5.56 kcal mol^{-1} due to low directionality of Pt−O and Pt−H bonds that, in turn, arises from high contribution of diffuse orbitals into bonding in Pt oxo complexes (see discussion of the nature of bonding below). Formation of **8** is strongly exergonic with ΔG_{298} = −66.59 kcal mol^{-1} with respect to individual **2** and H_2.

The last stage of the interaction involves migration of the agostic hydrogen to the hydroxide ligand, to give a water molecule. Since the agostic hydrogen is located trans to OH in **8**, this transition involves its long travel in addition to breaking of C_{ipso}−H bond and reorganization of Pt interaction with the aromatic ring. Our attempts to locate a hydride structure along the H "travel" pathway have failed. In contrast, we found that the agostic complex **8** and hydrato complex **9** are bridged by transition state **TS(8−9)** (see Figure 7), which presents a distorted square pyramid with apical H atom. Transition state **TS(8−9)** leads to an activation barrier of 20.40 kcal mol^{-1}. Notwithstanding the fact that this barrier lies far below the reactants on the energy scale, it presents the apparent activation barrier for hydrogen activation in acetone solution, in agreement with the experimentally observed reaction time. The agostic complex **8** is expected to be quite stable with a half-life on the order of 1.4 h.

Although water interaction with Pt in complex **9** has an attractive nature, it is not strong enough to overcome solvation and entropy effects. Thus, in acetone solution at room temperature, complex **9** undergoes water dissociation (ΔG_{298}=−2.33 kcal mol^{-1}) followed by acetone coordination (ΔG_{298} = −4.68 kcal mol^{-1}).

In conclusion, dihydrogen oxidation by the Pt-oxo complex **2A** follows quite a complex mechanism, which involves mandatory acetone dissociation, formation of a C−H agostic oxo complex, and a hydride-like transition state for the consequent hydrogen transfer.

d. Water Activation. Terminal oxo complexes are implicated as key intermediates in the artificial catalytic oxidation of water to dioxygen, the mechanism of which is a subject of numerous

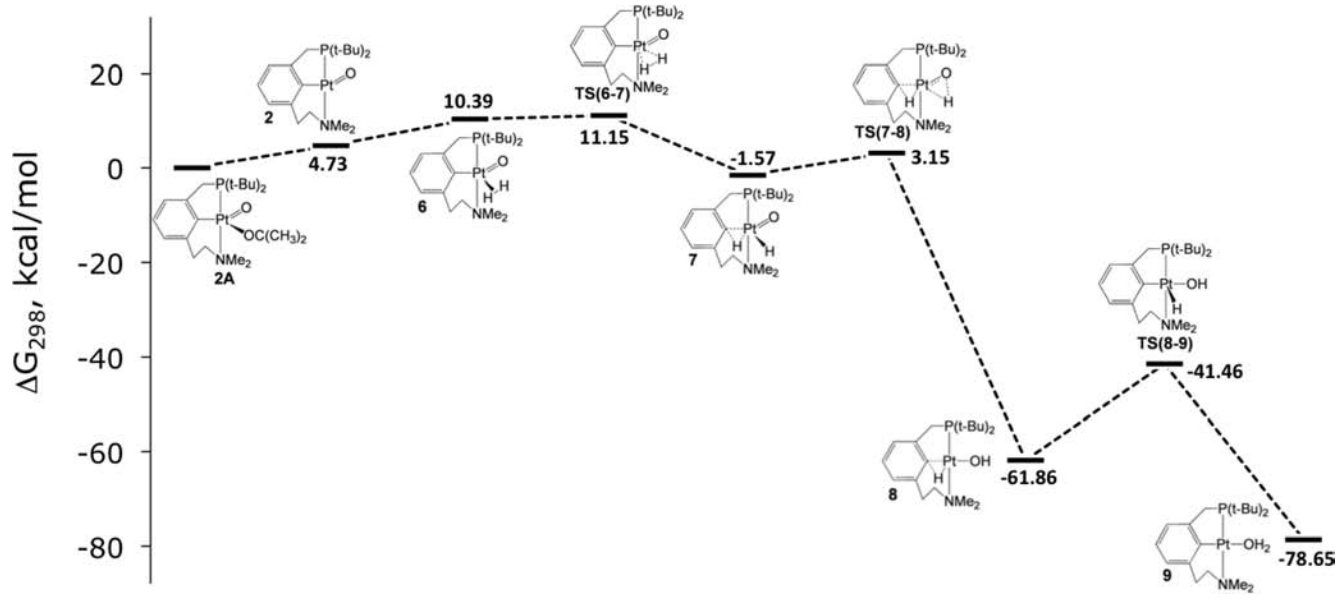

Figure 7. Reaction profile for H_2 oxidation by complex **2A**. All the complexes retain positive charge +1.

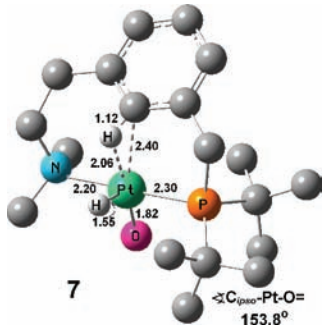

Figure 8. Optimized geometry of agostic hydrido complex **7**. Hydrogen atoms, except of those bound to Pt, are omitted for clarity.

theoretical and experimental studies,[54] although the nature of the step leading to the generation of dioxygen is under discussion.[1,55] In this context, it is desirable to know how a late TM terminal oxo complex reacts with water. In our previous publication,[5] the direct observation of water activation by a terminal oxo complex and trapping of the product of such activation was reported for the first time. It was shown that when an excess of water was added to **2**, the new dihydroxo Pt(IV) complex **4** was immediately formed (reaction 6 in Scheme 2). DFT calculations show that the overall reaction 6 is thermodynamically favorable (Scheme 6). In this context, understanding of the mechanism of water activation by the Pt-oxo complex can not only shed light on the electronic structure and reactivity of the complex itself but also is interesting as a model of water activation by late transition metal complexes suggested as intermediates in various catalytic processes.[56]

Scheme 6. Overall Reaction Energy (in kcal mol^{-1}) for Water Activation by Complex **2** in Acetone Solution

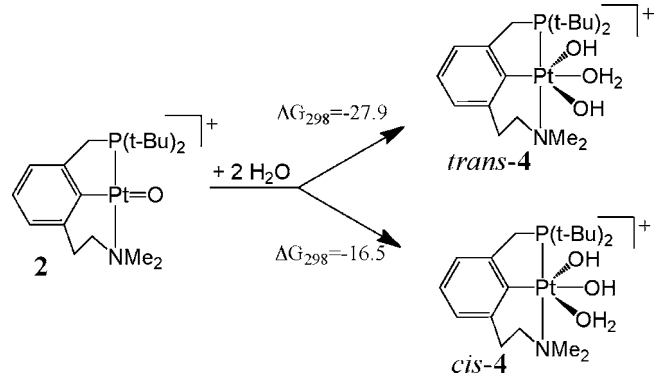

Interaction of **2** with a water molecule to give the dihydroxo PCN−$Pt(OH)_2$ complex is exergonic by $\Delta G_{298} = -19.52$ kcal mol^{-1}. Acetone displacement by water in complex **2A** with formation of complex **2-H_2O** is only slightly endergonic, as discussed above. The simplest reaction route, which consists of a direct H-transfer followed by trapping of an additional water molecule, is thermodynamically prohibitive at mild reaction conditions (Figure S5 in Supporting Information). However, water molecules[57] or other Lewis bases[58] often facilitate hydrogen transfer by formation of hydrogen bonds. Therefore, microsolvation with water would allow to avoid an intermediate oxidative addition stage. Interaction of complex **2** with two water molecules to give complex **4** is thermodynamically favorable with *trans*-**4** being 11.4 kcal mol^{-1} more stable than *cis*-**4** (Scheme 6). As coordination of two water molecules to the electron rich Pt-oxo complex is not possible (see above), the second water molecule could bind by hydrogen bonds to both oxo and coordinated H_2O ligands, thus providing a bridge for hydrogen transfer by formation of a Zundel-like transition

(52) (a) Autschbach, J.; Le Guennic, B. *Chem.—Eur. J.* **2004**, *10*, 2581. (b) Autschbach, J. *Coord. Chem. Rev.* **2007**, *251*, 1796.
(53) In the gas phase, complex **8**, when formed, has enough energy to overcome the following activation barrier; however, in solution the excessive energy is immediately spread over the solvation shell so that complex **8** presents a resting state on the potential energy surface.
(54) (a) Yang, X.; Baik, M.-H. *J. Am. Chem. Soc.* **2006**, *128*, 7476–7485. (b) Hurst, J. K. *Coord. Chem. Rev.* **2005**, *249*, 313–328. (c) Elizarova, G. L.; Zhidomirov, G. M.; Parmon, V. N. *Catal. Today* **2000**, *58*, 71–88. (d) Binstead, R. A.; Chronister, C. W.; Ni, J.; Hartshorn, C. M.; Meyer, T. J. *J. Am. Chem. Soc.* **2000**, *122*, 8464–8473.
(55) (a) Alstrum-Acevedo, J. H.; Brennaman, M. K.; Meyer, T. J. *Inorg. Chem.* **2005**, *44*, 6802–6827. (b) Betley, T. A.; Wu, Q.; Van Voorhis, T.; Nocera, D. G. *Inorg. Chem.* **2008**, *47*, 1849–1861. (c) Hurst, J. K.; Cape, J. L.; Clark, A. E.; Das, S.; Qin, C. *Inorg. Chem.* **2008**, *47*, 1753–1764. (d) Romain, S.; Vigara, L.; Llobet, A. *Acc. Chem. Res.* **2009**, *42*, 1944–1953. (e) Conception, J. J.; Jurss, J. W.; Brennaman, M. K.; Hoertz, P. G.; Patrocinio, A. O. T.; Iha, N. Y. M.; Templeton, J. L.; Meyer, T. J. *Acc. Chem. Res.* **2009**, *42*, 1954–1965.

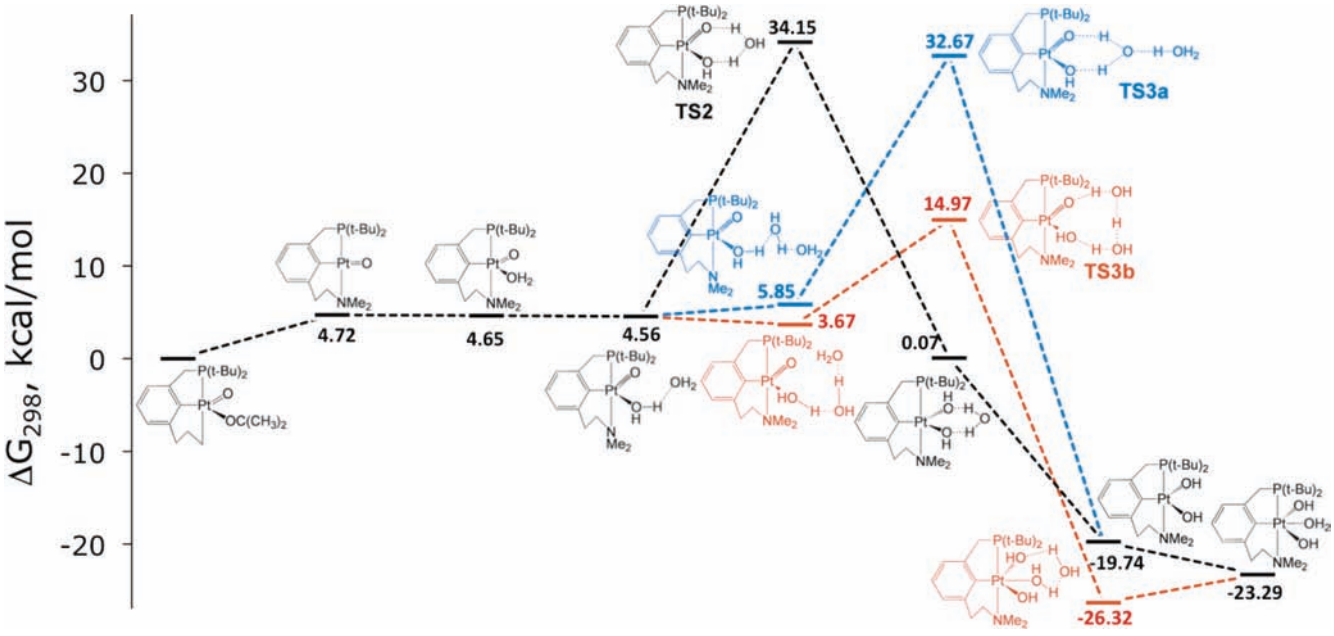

Figure 9. Reaction profiles for water activation in presence of two (black line) and three (blue and red lines) water molecules involved in the hydrogen transfer. All the complexes retain positive charge +1.

state.[59] High proton mobility in water media is attributed to existence of such structures.[60]

Simulations of hydrogen bonding in water clusters and protonated water clusters has attracted much attention in recent years.[61] Previous quantum chemical studies have shown the necessity of large basis sets for accurate treatment of hydrogen bonds.[62,63] The computational method implied in the present work is not accurate enough for this aim. Particularly, our test calculations showed the H-bond length in the water dimer is 0.065 Å shorter and the H−O···H bond angle is up to 11° larger in comparison with CCSD(T)/A'VTZ geometries[62] while the strength of the hydrogen bond was only 0.62 kcal mol^{-1} weaker than that calculated using the accurate W2 method[64] (see Table S1 in Supporting Information). In contrast, for the Zundel cation $(H_5O_2)^+$ we got a surprisingly good geometry, but interaction energy was underestimated by 6.49 kcal mol^{-1}. Nonetheless, as we are interested in relative energies of H-bonded complexes along reaction pathways rather than in absolute interaction energies, we believe that our energetic results are reliable, whereas our geometric data related to hydrogen bonds are valuable only in comparison with each other.

Reaction profiles for H_2O activation assisted by microsolvation with water are shown in Figure 9. Formation of the water network bound to the initial Pt oxo complex proceeds virtually isergonically on the calculated ΔG_{298} PES. As expected, significant (23.30 kcal mol^{-1}) lowering of the activation barrier with respect to the direct water activation pathway was observed when including one bridging water molecule in the model. However, transition state **TS2** leads to the barrier $\Delta G^{\ddagger}_{298}$ = 34.15 kcal mol^{-1}, still too high for the room temperature reaction. Addition of an explicit water molecule in the outer coordination sphere of the complex does not assist the interaction; the transition state **TS3a** is only 1.48 kcal mol^{-1} below **TS2**. Both transition states **TS2** and **TS3a** lead to the hydrated *trans* dihydroxo complex with trapping of an additional water ligand to follow. Formation of complex **4** in the large excess of water applied in the experimental conditions is accompanied by reorganization of its solvation sphere (see above). However, since this reorganization causes small changes in energy and has no effect on the kinetics of water activation, here we consider *trans*-**4** as a final product of the interaction.

When a second water molecule directly participates in hydrogen transfer (**TS3b**) the resulting activation barrier becomes only 14.97 kcal mol^{-1}, well consistent with the room temperature reaction. This mechanism suggests that reaction 6 is third order with respect to water, in accordance with the experimentally observed large excess of water needed for the reaction to occur. Unlike the transition states discussed above,

(56) (a) Labinger, J. A.; Bercaw, J. E. *Nature* **2002**, *417*, 507–513. Oxidation of Pt(II) to Pt(IV) by O2 in methanol to form a Pt(IV)(OMe)(OH) complex was reported: (b) Rostovtsev, V. V.; Labinger, J. A.; Bercaw, J. E.; Lasseter, T. L.; Goldberg, K. I. *Organometallics* **1998**, *17*, 4530–4531.
(57) (a) Iron, M. A.; Ben-Ari, E.; Cohen, R.; Milstein, D. *Dalton Trans.* **2009**, 9433–9439. (b) Lundin, A.; Panas, I.; Ahlberg, E. *J. Phys. Chem. A* **2007**, *111*, 9080–9086. (c) Liang, Y.; Zhou, H.; Yu, Z.-X. *J. Am. Chem. Soc.* **2009**, *131*, 17783–17785. (d) Jörgensen, S.; Kjaergaard, H. G. *J. Phys. Chem. A* **2010**, *114*, 4857–4863. (e) Fellah, M. F.; Onal, I. *J. Phys. Chem. C* **2010**, *114*, 3042–3051.
(58) Li, F.; England, J.; Que, L., Jr. *J. Am. Chem. Soc.* **2010**, *132*, 2134–2135.
(59) Zundel, G.; Metzger, H. *Z. Phys. Chem.* **1968**, *58*, 225.
(60) Vendrell, O.; Meyer, H.-D. *Phys. Chem. Chem. Phys.* **2008**, *10*, 4692–4703, and references herein.
(61) For recent review see, for example: (a) Sharp, K. A.; Vanderkooi, J. M. *Acc. Chem. Res.* **2010**, *43*, 231–239. (b) Malenkov, G. *J. Phys.: Condens. Matter* **2009**, *21*, 283101/1–283101/35. (c) Yagasaki, T.; Saito, S. *Acc. Chem. Res.* **2009**, *42*, 1250–1258. (d) Paesani, F.; Voth, G. A. *J. Phys. Chem. B* **2009**, *113*, 5702–5719. (e) Vener, M. V.; Librovich, N. B. *Int. Rev. Phys. Chem.* **2009**, *28*, 407–434. (f) Pluth, M. D.; Bergman, R. G.; Raymond, K. N. *Acc. Chem. Res.* **2009**, *42*, 1650–1659.
(62) Halkier, A.; Koch, H.; Jörgensen, P.; Christiansen, O.; Nielsen, I. M. B.; Helgaker, T. *Theor. Chem. Acc.* **1997**, *97*, 150–157.
(63) (a) Evdokimov, A.; Kalb (Gilboa), A. J.; Koetzle, T.; Klooster, W.; Martin, J. M. L. *J. Phys. Chem. A* **1999**, *103*, 744–753, and references herein. (b) Lundin, A.; Panas, I.; Ahlbergt, E. *J. Phys. Chem. A* **2007**, *111*, 9080–9086. (c) Boese, A. D.; Martin, J. M. L.; Klopper, W. *J. Phys. Chem. A* **2007**, *111*, 11122–11133.
(64) Martin, J. M. L.; De Oliveira, G. *J. Chem. Phys.* **1999**, *111*, 1843.
(65) Pedersen, B. *Acta Crystallogr.* **1974**, *B30*, 289–291.

Table 4. Effect of Microsolvation on the Calculated Apparent Activation Barrier for Water Activation (*n* is the Number of Water Molecules Involved in the Interaction at the Rate Determining Step)

n	1	2	3	3
TS	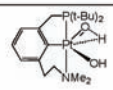	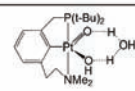	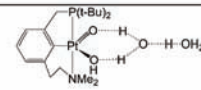	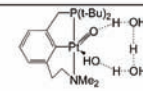
	TS1	**TS2**	**TS3a**	**TS3b**
$\Delta G^{\ddagger}_{298}$	57.44	34.15	32.67	14.97
Water framework	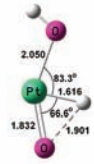		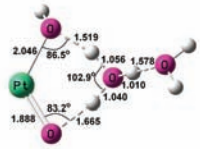	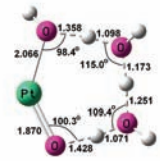

TS3b directly yields solvated *trans*-**4** as a kinetic and thermodynamic product.

Thus, the height of the activation barrier strongly depends on the structure and composition of the water network. A similar effect was previously observed in other hydrogen transfer reactions.[57a,b] The high efficiency of a water dimer as a bridge was attributed to geometric configuration of the transition state. The transition states for water activation obtained in the present work are summarized in Table 4, together with their important geometric parameters and corresponding apparent activation barriers. Indeed, our results indicate that H···O···H bond angles in the coordinated water dimer in transition state **TS3b** are quite close to 120°, the value expected for a 3-coordinated O atom, ∠Pt═O···H is close to ∠HOH in a water molecule (104.45°), while the O···H···O bond angles are close to linearity, the characteristic feature of the hydrogen bond from a donor water molecule. Therefore, breaking of three O−H bonds and formation of three new O−H bonds easily proceeds and results in an early transition state, i.e. the geometry of **TS3** is close to that of the reactant (Pt═O bond of 1.870 vs 1.809 Å in **2-H_2O**, Pt−OH_2 bond of 2.066 vs 2.344 Å, and ∠H_2O−Pt═O of 136.7 vs 158.1°, respectively). Only two O−H bonds are broken and two new O−H bonds are formed in transition state **TS2**. However, the geometry of **TS2** is characterized by much higher stress in the valence angles of the O atoms (∠Pt−O−*H* = 89.8°, ∠H···O···H = 103.3° for the three-coordinated O, ∠Pt═O···H = 91.0° for the two-coordinated O). Most importantly, the ∠H_2O−Pt═O is bent up to 109.7° in **TS2**. That hinders hydrogen transfer and results in a late transition state (longer Pt═O bond, 1.915 Å, shorter Pt−OH_2 bond, 2.056 Å, and moving H atoms are closer to their final positions than in **TS3b**). Formation of an additional hydrogen bond with an explicit water molecule from the second coordination sphere in **TS3a** causes some weakness of the H-bonds involved into the hydrogen transfer. That is immediately reflected by increased stress in the oxygen valence angles, by further movement of the transition state geometry toward that of the product, and by a resulting increase in the activation barrier.

Summarizing, the results presented in this subsection indicate that direct dissociation of a water molecule in the inner coordination sphere of complex **2-H_2O** is thermodynamically strongly unfavorable. Water activation by the Pt oxo complex assisted by microsolvation proceeds mainly due to the highly polar nature of the reactants.

Scheme 7. Key Orbital Interactions in (a) Planar and (b) Bent Complex **2**

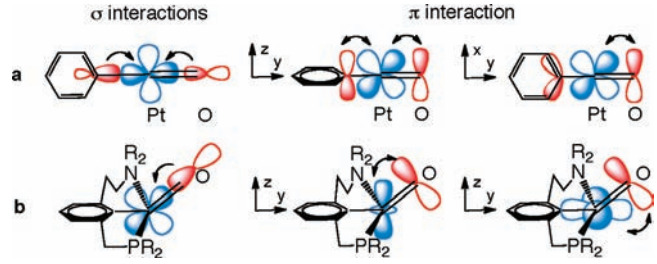

7. Nature of Bonding in the Pt−Oxo Complex

Intrinsic instability of terminal oxo complexes of electron rich transition metals is traditionally attributed to repulsive π interaction between p orbitals of the oxo ligand and occupied metal d orbitals. From Scheme 1 one can see that square planar d^6 TM complexes should be more stable than octahedral complexes. However, the phenyl ligand *trans* to the terminal oxygen in complex **2** intensifies the repulsion (Scheme 7a). In our previous publication,[5] we had shown that bending of the complex decreases these unfavorable interactions. Deviation from a perfect geometry presents a common feature of late TM oxo complexes,[4] thereby diminishing antibonding interactions with other π donor ligands. Figure 10 shows the dependence of Pt d orbital occupations on the C_{ipso}−Pt-O bond angle in complex **2** revealed by NBO analysis. In the planar complex, strong repulsion of the d_{yz} orbital with π orbitals of the phenyl and oxo ligands causes partial excitation of its electron density into diffuse 6s and 6p orbitals. Bending of the complex results in relaxation of the π repulsion and in O → d_{yz} σ donation, accompanied by increase of electron density on the d_{yz} orbital (Scheme 7,b). The π interaction splits into two components in the bent complex, so that both Pt d_{Z^2} and $d_{x^2-y^2}$ orbitals become involved in the repulsive interaction. Such changes in the Pt electronic structure result in stabilization by 17.6 kcal mol^{-1} at $\angle C_{ipso}-Pt-O \approx 140°$, in agreement with the optimized geometry of complex **2** ($\angle C_{ipso}-Pt-O = 138.2°$). The Pt−O and Pt−$C_{ipso}$ bond lengths shorten from 1.855 to 1.811 and from 2.003 to 1.985 Å, respectively, upon C_{ipso}−Pt−O bending from 180 to 138.2° while Pt−P and Pt−N bonds remain virtually untouched. This once again demonstrates that bending of the complex is due to the mutual repulsion of the phenyl and oxo ligands in *trans* position to each other. Further bending causes

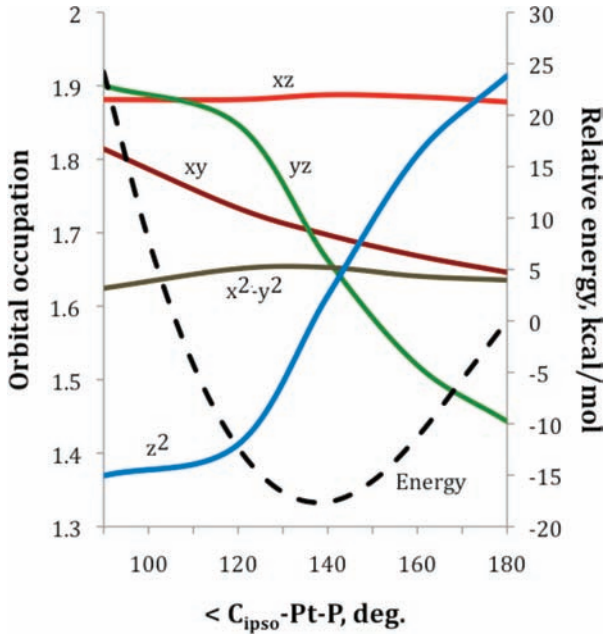

Figure 10. Influence of bending on Pt d orbital occupations and on relative energy of complex **2**.

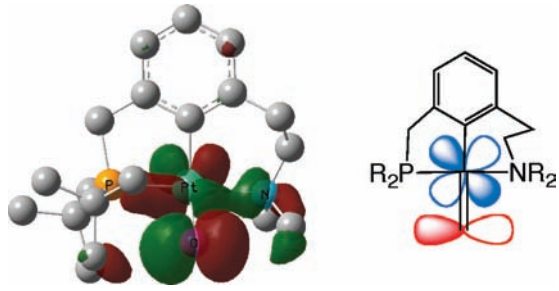

Figure 11. Contour plot and schematic representations of the highest occupied orbital of complex **2**.

strong destabilization of the complex owing to increased O → d σ donation and O p_π → Pt d_{yz} repulsion.

Occupation of the Pt═O π* orbital, the HOMO of the complex (Scheme 1 and Figure 11), presents another consequence of the large d-electron count. This orbital has a strongly repulsive character that, together with the repulsion between occupied Pt and O orbitals of π symmetry, brings about localization of electron density on the O atom. Both NBO and Mayer bond population analyses characterize Pt═O overlap population as a single bond. In addition, Mayer energy decomposition shows that the ionic component of the bonding is as large as the covalent component in the Pt═O interaction. So, the nature of the Pt-oxo bond could be represented as a resonance Pt═O ⇔ Pt^+-O^-. High polarity of the Pt═O bond manifests itself in the mechanisms of chemical reactions discussed above. Particularly, complex **2** is inactive in activating of the nonpolar C−H bonds in the coordinated acetone molecule. In the reaction of hydrogen oxidation the oxo ligand appears to be less reactive than phenyl with respect to the coordinated hydrogen (leading to an agostic C−H intermediate) in complex **6** (Figure 7). Similarly, direct inner-sphere hydrogen transfer in the reaction of water oxidation is energetically strongly unfavorable (Figure S5, Supporting Information) while the most probable reaction pathway assisted by outer-sphere water molecules involves hydrogen bonding as a key interaction (Figure 9) and thus it is mostly polar in nature.

Table 5. Key Bond Lengths and Wiberg Bond Indexes in Complexes **1**, **2** and **2A**

	bond length, Å			Wiberg bond index (WBI)		
	1	**2**	**2A**	**1**	**2**	**2A**
Pt═O		1.811[a]	1.811		1.310	1.292
Pt−C_{ipso}	1.977	1.985	2.017	0.869	0.778	0.720
Pt−N	2.165	2.222	2.228	0.262	0.302	0.298
Pt−P	2.260	2.291	2.296	0.706	0.703	0.689

[a] For comparison, the Pt(IV)═O bond length in the POM-stabilized $K_7Na_9[Pt(O)(H_2O)(PW_9O_{34})_2]$ complex was measured to be 1.720 Å while the average Pt(IV)−O single bond distance is 1.992 Å.[4,4a]

All late TM oxo complexes characterized so far are stabilized by electron-withdrawing ligands. For instance, stability of the d^6 NaRe(O)$(PhCCPh)_2$ complex[4d] is attributed to rhenium → acetylene π backbonding. Partial transfer of the excessive electron density to π* W = O orbitals is responsible for the stabilization of terminal oxo complexes of the group 10 and 11 elements embedded into the polytungstate ligand environment.[4,4a−c] Phenyl, amine and phosphine groups of the pincer ligand in complex **2** are known as strong σ donors. A huge (∼20 eV) energy gap between occupied orbitals of $Pt{=}O^{2+}$ and empty orbitals of phenyl makes Pt → phenyl backdonation impossible. Charge decomposition analysis confirms that such backbonding is virtually absent in complexes **1** and **2**. Due to the presence of empty d orbitals on the phosphorus atom, the phosphine group could serve as a weak π acceptor. Indeed, charge decomposition analysis reveals small (0.019 electron) Pt → P, N backdonation in complex **1**, which increases to 0.054 and 0.084 electron in **2** and **2A**, respectively. Such small backdonation effect arises from the geometric structure of the complex since the main repulsive interaction occurs in the yz plane (Scheme 7), axial to the Pt−P bond.

Circumstantial examination of the wave functions of complexes **1**, **2** and **2A** reveals that the main stabilization of the Pt═O unit is achieved by significant transfer of the excessive electron density from compact, low-lying, Pt 5d orbitals to more diffuse 6s and, especially, to 6p orbitals. Detailed Mulliken population analysis yields decrease of Pt 5d orbital occupations in the above series from 7.046 to 6.799 and to 6.792. In contrast, the Pt 6s orbital occupation increases from 1.733 in **1** to 1.748 in **2** and to 1.743 in **2A**. Occupation of the Pt 6p orbitals increases even stronger (from 5.133 to 5.205 and to 5.210, respectively). Moreover, the electron density on diffuse Pt p orbitals rises by 0.101 and by 0.135 when moving from **1** to **2** and to **2A**, correspondingly (see also electron density counter plots, Figure S6 in Supporting Information). While the presented values themselves have limited physical meaning, they qualitatively explain the upfield chemical shift upon Pt-oxo bond formation found for C_{ipso} atom both theoretically and experimentally, the relatively low-field ^{195}Pt NMR signal observed for the Pt oxo complex and the strong deviation of calculated ^{195}Pt chemical shifts of **2** and **2A** from a linear relationship with the Pt atomic charge (Figure 5). Involvement of the diffuse orbitals in bonding causes elongation of Pt bonds with P, N and, especially, with C_{ipso} atoms (Table 5). It is accompanied by weakness of Pt−C_{ipso}, as indicated by changes of corresponding WBIs. Notably, acetone coordination in complex **2** elongates and weakens mainly the Pt−C_{ipso} bond while Pt═O interaction is much less affected. Such stabilization effect seems to be unlikely in late TM oxo complexes stabilized by electron withdrawing ligands.

8. Conclusions

The recently reported $[(PCN)Pt{=}O]^+$ complex[5] **2** presents a unique example of a terminal d^6 oxo complex not stabilized by electron-withdrawing ligands. It was characterized by various physicochemical methods in acetone solution but, due to its only moderate stability, single crystals suitable for X-ray diffraction were not available. With the purpose to get a more comprehensive and detailed picture on the properties of the complex, we performed extensive DFT study of its geometric and electronic structure and reactivity.

All of the complexes reported in ref 5 were fully characterized by multinuclear NMR spectroscopy. To get a link between experimentally synthesized complexes and their structure and composition in acetone solution, we performed relativistic ECP and all-electron calculations of ^{13}C, ^{1}H and ^{195}Pt chemical shifts for complexes **1**−**4** in absence and in presence of ancillary ligands. The calculated ^{13}C and ^{1}H shielding tensors were scaled with respect to accurate coupled cluster results at the basis set limit and to experimental data, while for ^{195}Pt NMR only experimental data were used for scaling. Our overall results for ^{13}C and ^{1}H NMR chemical shifts are in very good agreement with the experimental data, thus confirming the atomistic structure of complex **2**. More detailed information on the electronic structure and composition of the complexes could not be retrieved from calculated ^{13}C and ^{1}H chemical shifts due to low sensitivity. In contrast, the ^{195}Pt chemical shift is very sensitive to electronic structure and ligand environment. Fortunately, explicit modeling of a solvent molecule in the first coordination sphere together with accounting of bulk solvent effect in the form of a continuum model appears to be accurate enough for ^{195}Pt NMR calculations in pure acetone solution. This is not the case for water or mixed acetone−water solutions, where hydrogen bonds with second-sphere water molecules strongly influence calculated chemical shifts. Comparison of the calculated ^{195}Pt NMR chemical shifts with the measured one indicates that $[(PCN)Pt{=}O]^+$ complex adopts form **2A** with one weakly coordinated solvent molecule in acetone solution. This conclusion is confirmed by thermodynamic data.

Chemical transformations of the coordinated acetone molecule, coordination of other ancillary ligands present in the reaction mixture, and protonation of the Pt-oxo group at the experimental conditions described in ref 5 are excluded based on thermodynamic or kinetic considerations. All these factors, together with steric protection of the complex against dimerization by a bulky ligand environment[5] allow complex **2** to be identified. On the other hand, protonation of the complex in acidic media is predicted to be strongly favorable.

Mechanistic study and electronic structure analysis show that reactivity of the Pt-oxo complex is determined by an excess of electron density on the metal center that strongly weakens the $Pt-C_{ipso}$ bond and, to a lesser extent, the Pt−P bond. The oxo O atom favors nucleophilic interactions rather than "soft" covalent bonding. Thus, oxygen insertion into the Pt−P bond in complex **2** has a very small activation barrier; the moderate stability of the complex stems from the presence of an acetone ligand. Destabilization of CO coordination in complex **2** by the acetone ligand plays a key role in the reaction of CO oxidation. Water activation by the Pt oxo complex proceeds via intermediate formation of a 8-membered ring involving the Pt-oxo group and three water molecules linked by hydrogen bonds. In all these reactions bonding of the oxo O with strong electrophiles presents the key interaction. In contrast, dihydrogen oxidation by complex **2** proceeds through intermediate formation of an agostic C−H complex followed by thermodynamically driven hydrogen transfer to oxo O. This indicates an inferior affinity of the terminal oxo toward "soft" covalent interactions in comparison with the phenyl group.

Hybrid DFT methods yield an open-shell ground state of complex **2**, at variance with the experimentally observed diamagnetism of the complex. In the present work we show that this is due to the well-known tendency of these methods to favor high-spin states. More accurate calculations using the recently published B2GP-PLYP double hybrid functional show that singlet and triplet states of complex **2** are isoenergonic at the basis set limit. Acetone coordination provides additional stabilization of the diamagnetic state of the complex.

Repulsive interaction between π orbitals of the oxo ligand and occupied metal d orbitals and presence of π-donor phenyl ligand in *trans* position should make d^6 Pt oxo complex unstable. The negligible π backdonation ability of the PCN ligand environment cannot delocalize the d electron count, as electron withdrawing ligands can do in the rare late transition metal oxo complexes published so far.[4] Detailed electronic structure analysis demonstrates that increase of the net Pt-oxo bonding is achieved by two main factors: (i) Bending of the terminal oxo ligand out of the plane of complex **2** allows for redistribution of electron density and partial release of π repulsion. (ii) Stabilization of the Pt=O unit is mainly achieved by significant transfer of the excessive electron density from compact low-lying Pt 5d orbitals to more diffuse 6s and, especially, to 6p orbitals, at the cost of weakness of other metal−ligand bonds. This effect is confirmed by the strong deshielding observed in experimental and, especially, in calculated ^{195}Pt NMR of complex **2**. Such excitation of electron density seem to be unlikely in late transition metal oxo complexes stabilized by electron-withdrawing ligands.

Acknowledgment. We thank the European Research Council (ERC 246837), The Israel Science Foundation, the MINERVA Foundation, and the Weizmann AERI (Alternative Energy Research Initiative) for financial support. D.M. and J.M.L.M. are the holders of, respectively, the Israel Matz Professorial Chair of Organic Chemistry and the Margaret Thatcher Chair in Chemistry.

Supporting Information Available: Performance of PBE0/pc-1 method in determination of energy and geometry of hydrogen bonds, optimized geometry of the $[(PCN)(acetone)Pt{=}O]^+$ complexes **2A**, unobserved acetone transformations in complex **2A**, details about NMR calculations, counter plots of electron density, and full references 4b, 4c, 12, 13 and 35. This material is available free of charge via the Internet at http://pubs.acs.org.

JA105197X